FINITE ELEMENT ANALYSIS OF VORTEX MACHINING PROBES

by

Mandar Dilip Vaidya

A thesis submitted to the faculty of
The University of North Carolina at Charlotte
in partial fulfillment of the requirements
for the degree of Master of Science in
Mechanical Engineering

Charlotte

2014

Approved by:

_____
Dr. Alireza Tabarraei

_____
Dr. Stuart Smith

_____
Dr. Harish Cherukuri

ABSTRACT

MANDAR D. VAIDYA. Finite element analysis of vortex machining probes. (Under the direction of DR. ALIREZA TABARRAEI and DR. STUART SMITH).

Vortex machining is a unique localized material removal process in which footprints of several nanometer in depth are obtained. It employs a resonating quartz tuning fork and a fiber attached on its upper tine. When submerged in a layer of slurry, tip of the fiber produces vortices in the medium. These vortices cause a localized material removal of the workpiece, also placed in the slurry. Machining process is complex and the rate of material removal is governed by a number of parameters, such as slurry depth, offset distance between fiber tip and workpiece, fiber length, exciting frequency of tuning fork, etc. Also the imperfections such as misalignment between fiber and fork tine can impact the fiber tip displacement.

The objective of this thesis is to study the factors that affect the displacement of the fiber tip, and to gain insights regarding maximizing the displacement of the fiber tip. Finite element analysis of the probe (assembly of the fork and fiber) is carried out to examine the impact of parameters such as fiber length, exciting frequency and imperfections on the tip displacement. Symmetric and anti-symmetric modes of longitudinal vibration of the fork are used to apply the loading in dynamic simulations. The finite element results predict that misalignments do not have a significant impact on the tip displacement. However, the imperfect bonding between fiber and fork can affect the fiber tip displacement. Furthermore, the results reveal that the glue between fiber and fork is an important factor

affecting the fiber tip displacement, and should be considered in the finite element models. The results obtained are consistent for both the symmetric and anti-symmetric loadings.

DEDICATION

I dedicate all of my work to my loving and caring parents. It would not have been possible to reach here without their constant support and encouragement.

ACKNOWLEDGMENTS

I would like to sincerely thank Dr. Alireza Tabarraei for letting me become part of his research group. His guidance, useful comments, and motivation helped me reach my goal of completing thesis. This work would not have been completed without invaluable guidance and motivation from Dr. Stuart Smith. Thank you for giving me an opportunity to work with you. I also would like to sincerely appreciate Jeffry Hunt for passing on his knowledge of vortex machining. I take this opportunity to express my deep gratitude to Dr. Harish Cherukuri for giving out his valuable time to serve on my thesis committee.

To all my friends both from the University and elsewhere, thanks for motivating and supporting me towards completion of my degree. It has been a very memorable journey spending quality time with you all.

TABLE OF CONTENTS

LIST OF TABLES

LIST OF FIGURES

CHAPTER 1: INTRODUCTION AND BACKGROUND

1.1 Introduction

Vortex machining is a localized material removal process in which footprints are brought about using a quartz tuning fork (QTF) and an attached fiber. The fiber is glued normally to the fork axis at one of its tines. Current passed through the fork using an existing electrode coating excites the QTF. This in turn sets the fiber into an oscillating motion. Figure 1.1 shows a schematic representation of the fork and the fiber assembly. The fiber end is submerged into a slurry, where such oscillating motions are put into use to induce vortices. Finally, the vortices cause a nanometer level surface removal of the workpiece, also immersed in the slurry.

Figure 1.1: A schematic representation of the QTF and the fiber attached on its upper tine

QTFs, which act as the resonators in vortex machining, are the most widely used sensors in scanning microscopes [1-3]. A QTF offers several advantages: Firstly, quartz is one of the most abundantly available minerals in the earth's crust and inexpensive. Billions of QTFs are made annually. They also possess frequency stability; i.e., the frequency of such tuning forks remains fairly constant even in varying temperature conditions over a

long period of time [4]. The quality factor (also known as Q-factor), which inversely represents internal mechanical losses resulting in loss of rate of energy, is also very high [5]. Higher the Q-factor, fewer is energy loss rate meaning that their oscillations damp out slowly. It is clear that QTFs offer a complete package and are thus used ubiquitously across a variety of industrial applications.

For example, detection of surface deposits from gaseous environments is pivotal for chemical processing industries. With a suitable electronic design, the QTFs are used for gas sensing technology [6]. On the similar lines, QTFs are conveniently used in biological applications to detect certain bacteria [7]. Quite often, QTFs are effective tools in detecting the fluid properties, such as viscosity, density, etc. [8-11].

In almost all of the applications discussed, the scanning technique is accomplished using atomic force microscopes (AFM), a special category of microscope, in which the QTFs may act as a resonator. In such applications, the QTFs are set to vibrate at their known natural frequencies. When they come into contact with a media, its interaction acts as damping source. This leads to a drop in the resonating frequency of QTFs. This change of frequency forms the foundation to uncover the quantity of interest, extracted using transducers [12].

Moreover, geometrical contour measurement or and surface detection can be performed using tuning forks. Bauza et al [13] developed a probe model (an assembly of a tuning fork and an attached fiber) for geometric feature measurements. The probe discussed in this thesis has been proposed initially for metrological applications. The fiber is attached coaxially to the upper tine of the fork with one of its end being extended along the tine length. The free end of the fiber acts as a ‘contact point’. Owing to sufficiently longer fiber

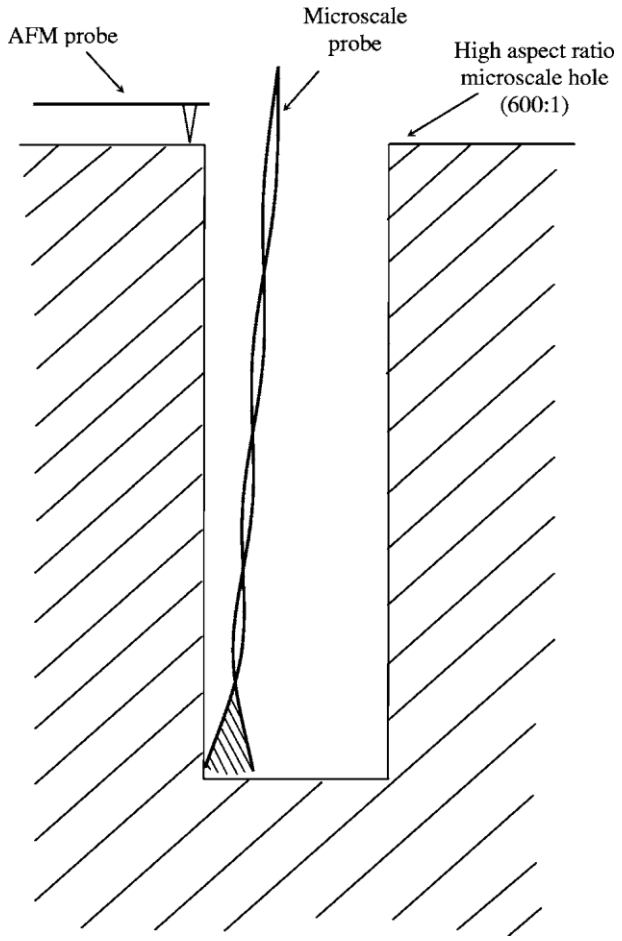

Figure 1.2: Schematic diagram for measurement of high aspect ratio holes, adopted from [13]

length, this contact point has a far extensive ‘reach’, enabling it especially to measure holes with aspect ratios as high as 700:1.

Another significant advantage of this technique is in a non-destructive measurement of such intricate features. In conventional AFM measurement, the cross-sections need to be chopped off for metrological purposes. Bauza et al has provided a new non-destructive modus operandi to fix this issue.

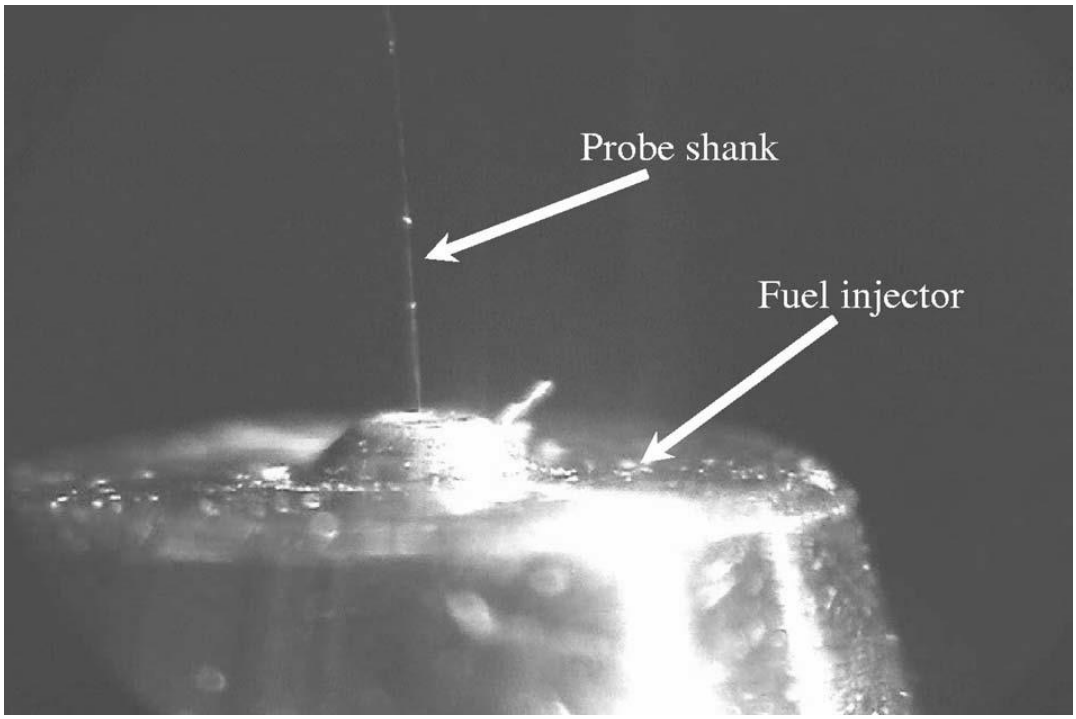

Figure 1.3: Photograph showing a 7 μm probe tip inside a 100 μm fuel injector hole, adopted from [13]

When a probe comes in contact with a feature, there is a dominant adhesive force acting between them. Hence, a static probe (no excitation of fork) is prone to sticking, leading to reduced repeatability and an increased measurement time. This explains the necessity of a vibrating system, which is able to put the tip inside a diesel engine fuel injector hole to accurately measure its diameter, as shown in figure 1.3 [13].

The dynamic probes have also been exercised in micro-robotic applications. Shane Woody et al. [14] performed experiments revealing effectiveness of these probes to sense specimens, pick them up to transport at a desired location. In this approach, a pair of static probes are positioned near the object to be moved. The adhesive forces cause the object to stick to the fiber. The robotic mechanism place the specimen at a desired position. Fork is then actuated triggering the fiber to vibrate. The vibrating motion causes the probe to

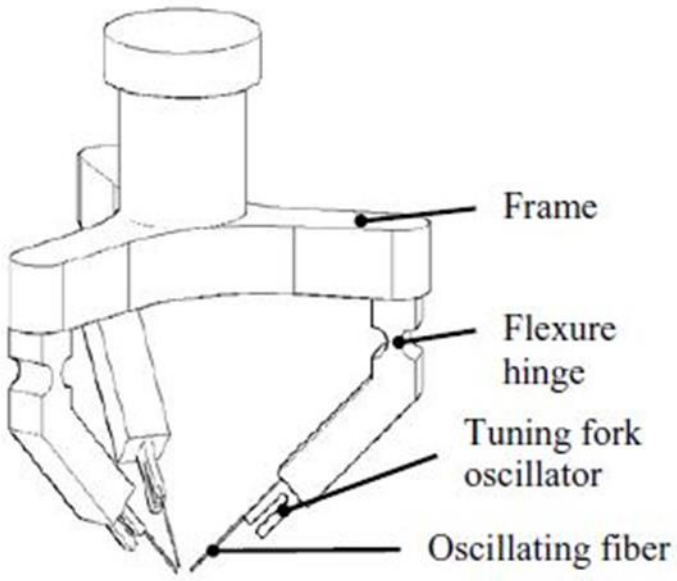

Figure 1.4: Schematic diagram of a three-fingered micro-robotic arm, adopted from [15]

overcome the adhesive forces, and thus setting it apart from the specimen.

A similar study had been carried out in the Center for Precision Metrology at the UNC Charlotte. Jacob Chesna et al.[15] and D. J. Hastings et al. [16] developed a micro-scale robotic system acting as a three fingered ‘grippers’ efficiently translating specimen. A simple schematic of the model is shown in the figure 1.4. It consists of a three fingered hand whose motions are precisely controlled. The probe is positioned at the end of each finger. Efforts are made to make identical probes, and each probe is excited by a single source to achieve a synchronous motion. The fingers are used to pick up and drop the specimen only. The displacement motion of the sample is achieved by a moving platform on which the sample is placed.

Nowakowski et al. [17] investigated a technique to monitor the amount of mass being lost in an electrolytic reaction using the probes with attached tungsten fibers. Such a method can be helpful to control the mass removal in electromechanical processes

employed in applications, such as etching. The tungsten wire serves as an anode in the reaction at which oxidation takes place. The loss of tungsten affects the dynamics of the model and a frequency alteration is reported. This change of frequency can be used as a parameter to precisely control the mass removal. The results of the system were validated by using a similar tungsten wire in alternative conventional arrangement of the electrolytic experiment being run for the same duration, and the mass of the wire measured before and after the test.

It is thus clear that the probes have been used in a wide variety of applications and in diverse fields. Nowakowski et al. [18] first examined their feasibility to determine if a material removal was possible. The tip of the fiber was allowed to oscillate in a slurry. The vibrations of the tip induced localized vortices in the slurry. These vortices, in turn, triggered a surface modification of the workpiece placed in the slurry. This unique process of a material removal came to be known as ‘vortex machining’. Significant advances have been made at the Center for Precision Metrology in the University of North Carolina at Charlotte to improve the process.

Figure 1.5 shows a schematic representation of the vortex machining process. The fork is excited using an electric charge. The free end of the fiber submerged in the slurry produces vortices. The workpiece is located on a moving platform. By controlling this position, vortices can be made to induce in a confined area. This helps achieve localized impressions on the workpiece.

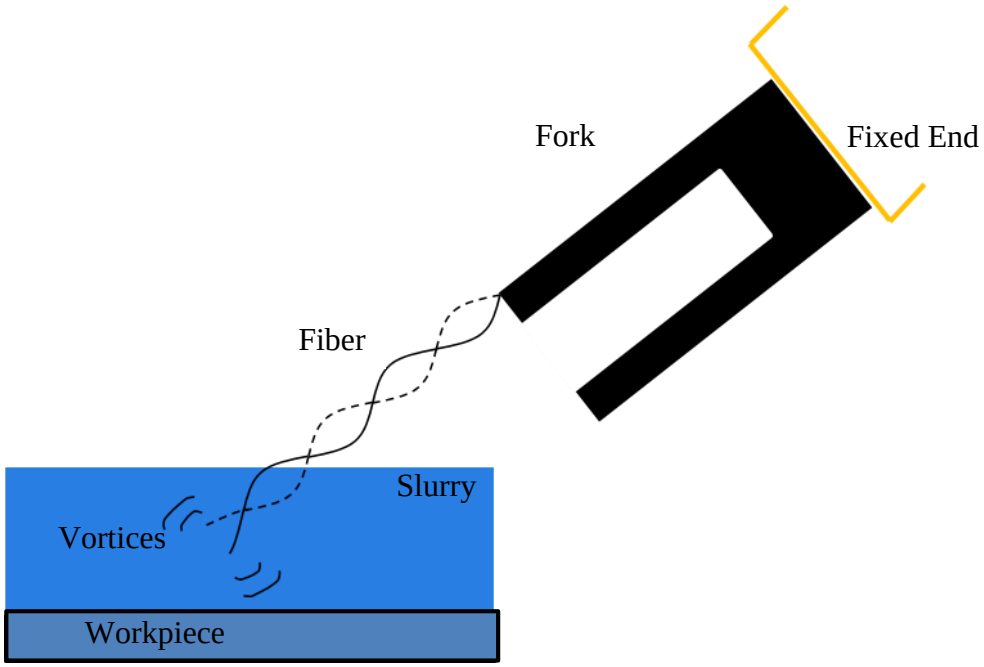

Figure 1.5: Schematic diagram for vortex machining

1.2 Experimental Set-Up

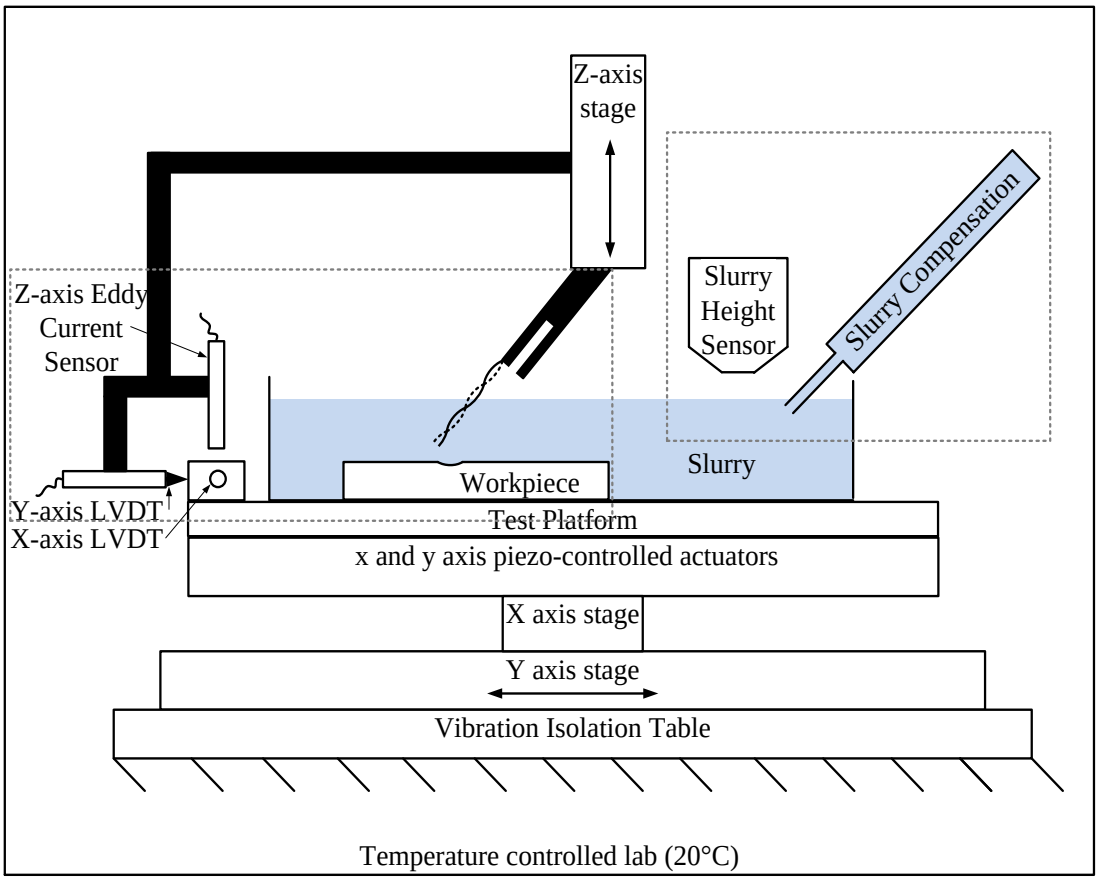

Figure 1.6: Schematic of vortex machining platform, adopted from [18]

Figure 1.6 shows the vortex machining platform. The workpiece submerged in a container filled with slurry is placed on a movable dais. It has a two degree of translating freedom. Precise advancement in each direction (X and Y) is manipulated through individually assigned stages, which are LVDT controlled. The position, after achieving a desired alignment, is locked. The probe is attached to a Z-axis stage perpendicular to X and Y axis to monitor the fiber tip and workpiece stand-off distance. The whole assembly is mounted on a vibration isolating table to eliminate external vibrating influences. The flow

of the slurry is constantly monitored and maintained. Figure 1.7 shows a photograph of the whole set-up.

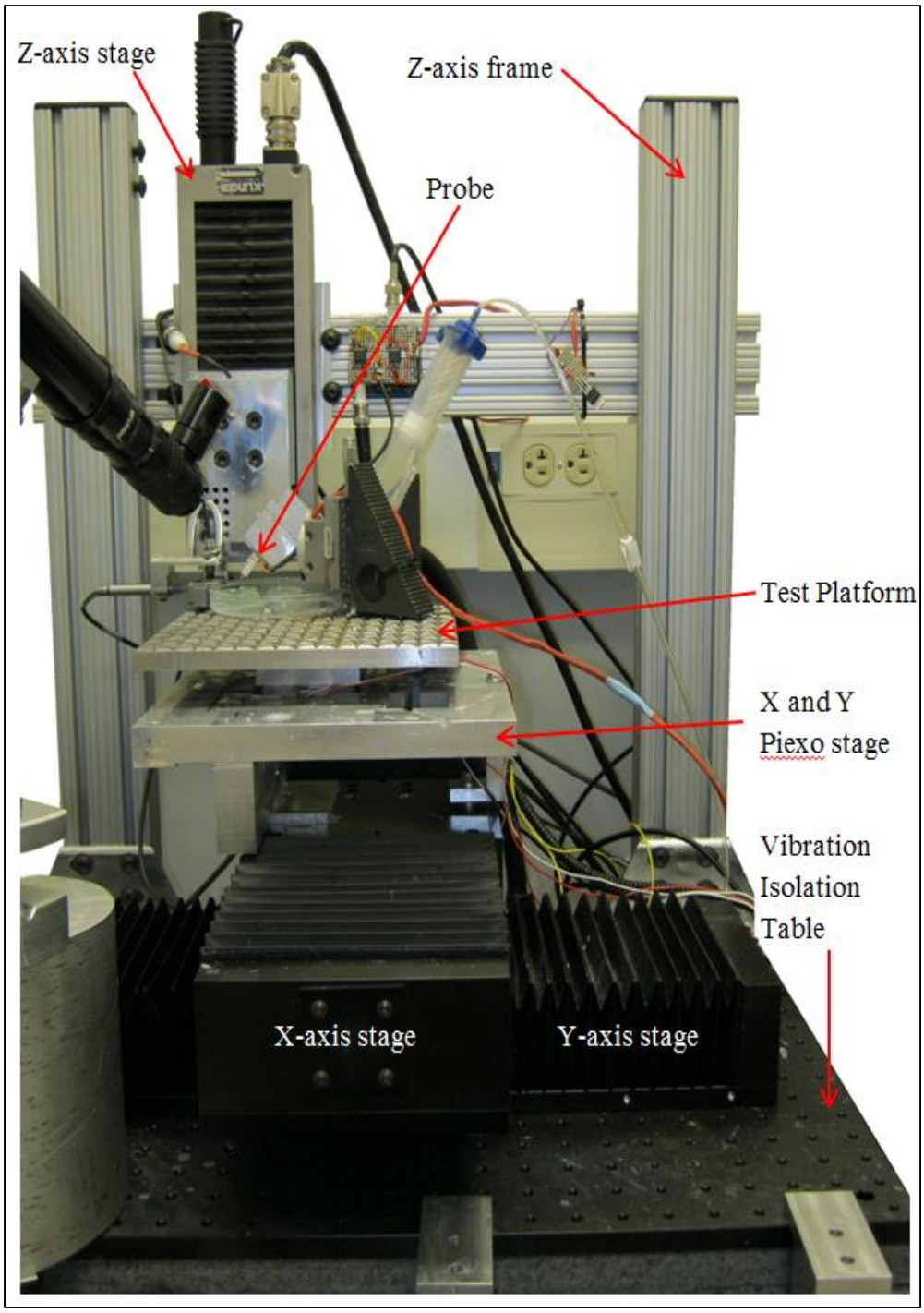

Figure 1.7: Actual experimental platform, adopted from [18]

In the vortex machining process, the rate of material removal is governed by a number of parameters:

1) Slurry depth

If the height of the slurry is too high, then the slurry itself would act as a damping medium reducing the tip displacement of the fiber. This would lessen the material removal.

2) Standoff distance between tip of the fiber and the workpiece

Increasing the distance between fiber and workpiece would ideally diminish the vortex strength undermining the degree of impression.

3) Frequency of vibration

The system, if vibrated at a resonance, would understandably oscillate with maximum amplitude, boosting the rate of machining.

4) Length of fiber

It is desirable to see if the length of fiber would have any impact on the system.

5) Effect of misalignment

Since the probes are so tiny, it is impossible to perfectly align the fiber (coaxial and symmetric placement) on the upper tine of the fork. It is thus vital to inspect the impact of such misalignments.

6) Type of slurry

Slurry type and particle size is likely to have some bearing on the volume of material removal rate.

7) Material to be machined

Clearly, different materials have different wear resistance. If a substance has a superior wear durability, yield from the process will be limited.

8) Other

There can be several parameters influencing the machining operation. Some of these factors include duration for which the tip is held at a certain location, tool wear (effect on fiber tip due to the abrasion with the slurry), and ambient temperature, etc.

1.3 Scope of This Thesis

Explicit finite element analysis of the probe is performed in this thesis. It is challenging to monitor the exact tip motion in experiments. Moreover, tiny geometry of the model makes it difficult to confirm if the effects such as misalignment have on the tip displacement. The focus of research is thus to maximize the tip displacement of the fiber and the parameters affecting it are factored in. Accordingly, out of the parameters mentioned above, three factors, i.e. frequency of vibration, fiber length, and misalignment, are investigated. Probes ranging from 3.20 mm to 3.80 have been numerically modeled and an optimized probe is analyzed further. The effects of misalignment on the amplitude of tip oscillations are studied. Furthermore, a tip displacement is inspected at a range of exciting frequencies of the fork. This frequency sweeping operation is performed on probes with and without glue coating.

There is a symmetric mode of vibration for the fork in which the tines move in the same direction normal to the tine length. On the other hand, an anti-symmetric vibration mode corresponds to the tines moving in opposing directions. Both the symmetric and anti-symmetric modes of vibration have been considered in this work for all of the three mentioned cases.

1.4 Outline of the Thesis

Chapter 2 describes the various modeling scenarios involved in the project. Material type and their properties for the given system is discussed in chapter 3. Chapter 4 illustrates the specifics of the finite element model. In chapter 5, results and parametric studies involved in the model with the symmetric mode of vibration have been depicted, while chapter 6 discusses the results and parametric studies for the anti-symmetric mode. Finally, chapter 7 concludes the work.

CHAPTER 2: MODELING SCENARIOS

The tuning fork probe model is built in Abaqus/Explicit. Figure 2.1 depicts the dimensions of the probe. The fiber diameter is 7 μm, while width of the fork measures 0.24 mm.

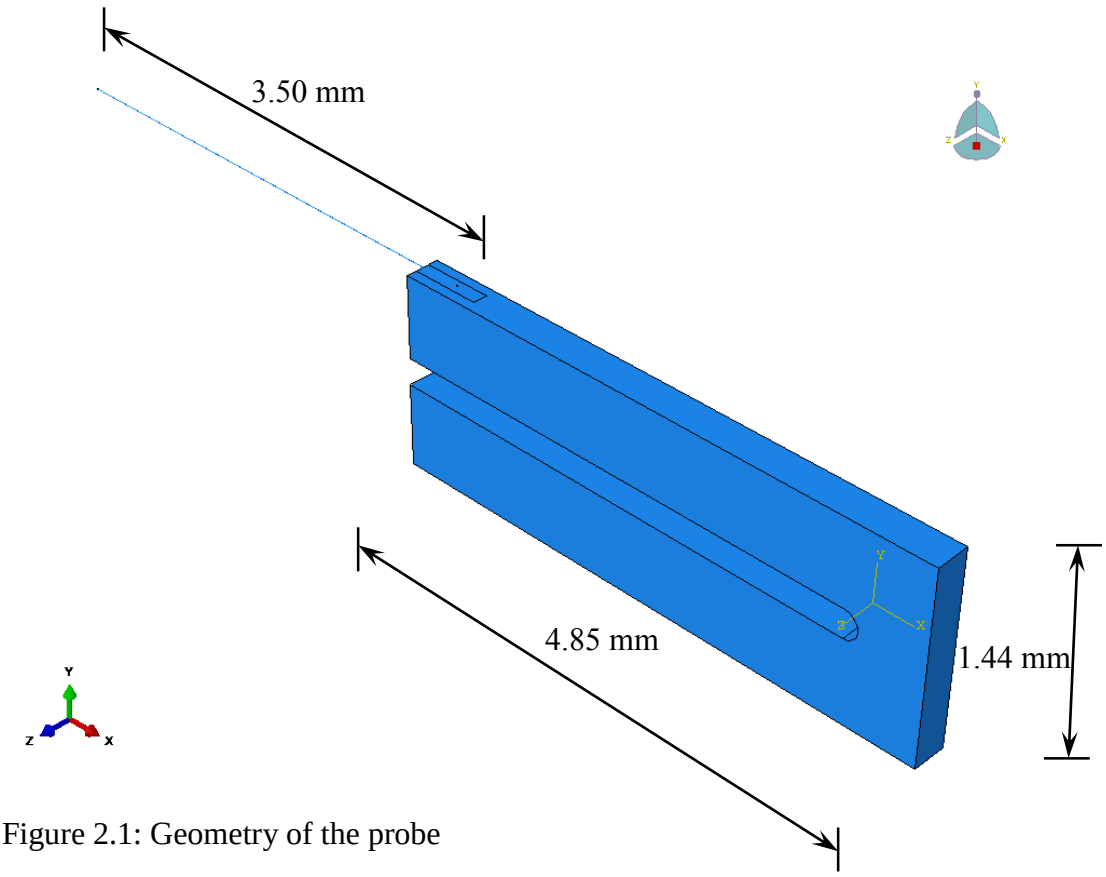

Figure 2.1: Geometry of the probe

Different modeling scenarios being considered in the thesis are discussed below:

1) Probes Exclusive of Glue

There can broadly be two categories within this analysis: 1) a perfect node-to-node connectivity, and 2) an imperfect contact. For this thesis, a model with a perfect connectivity and without layer of glue coating is first analyzed.

1.1) Probes Exclusive of Glue and a Perfect Connectivity

In this category, a probe with the fiber aligned coaxially on top of the upper tine of the fork (symmetric position) is initially considered. Apart from this, the fiber axis may be off-centered or skewed with respect to fork axis due to the small size of the assembly. The effect of misalignment on the tip displacement is thus studied. For this purpose, models with fibers located at offset, angular, offset-angular position with respect to axis of the fork along the tine direction have been developed, and studied. These positions have been illustrated in figures 2.2.

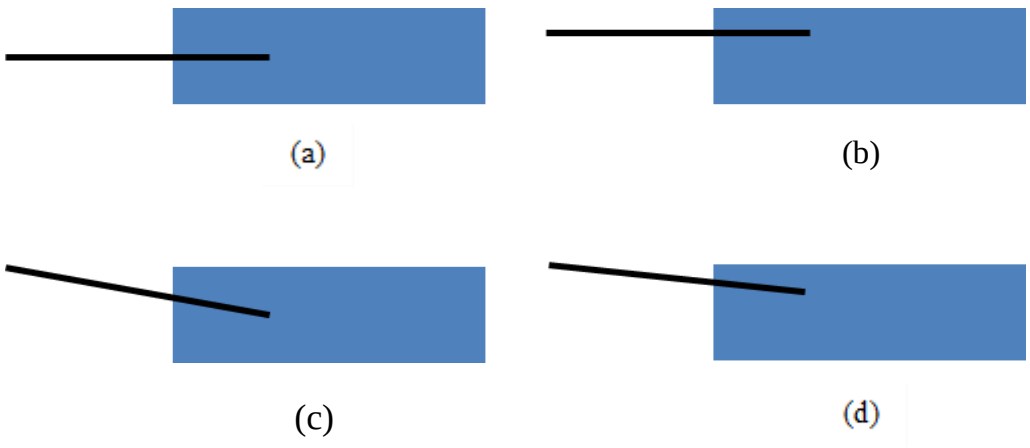

Figure 2.2: Illustration of different positions of the fiber with respect to fork, (a) depicts the symmetric position (b) denotes an offset position (c) shows a skewed position, and (d) indicates an offset-skewed position

Furthermore, models with changing offset positions of the fiber, namely 0.030 mm, 0.045mm, 0.060 mm, are built. The distances are referenced from the axis of fork. Similarly, differing angular positions of the fiber are also tested. The angles considered are 3°, 5°, and 7°.

1.2) Probes Exclusive of Glue and an Imperfect Contact

To model inadequate bonding between the fiber and the tuning fork, a second model of an imperfect contact has been implemented. In this case, some of the nodes along the line of contact are not merged. This mode of contact is also subdivided into two categories. In one such arrangement, random number of nodes along the line of contact are merged. The next model has all but the nodes just at the fork tine end being combined. The modeling arrangement can be clearly understood from the figures 2.3 (a) and (b) where the pink colored dots represent the number of nodes of both the geometries being merged.

2) Probes with Glue Coating

Lastly, a thin layer of glue has been sandwiched between the fork and the fiber. The thickness of the layer is suitably assumed as 1.2 μm to 'pass' the glue elements in aspect ratio. The fiber is assumed to be coaxially placed on the fork tine.

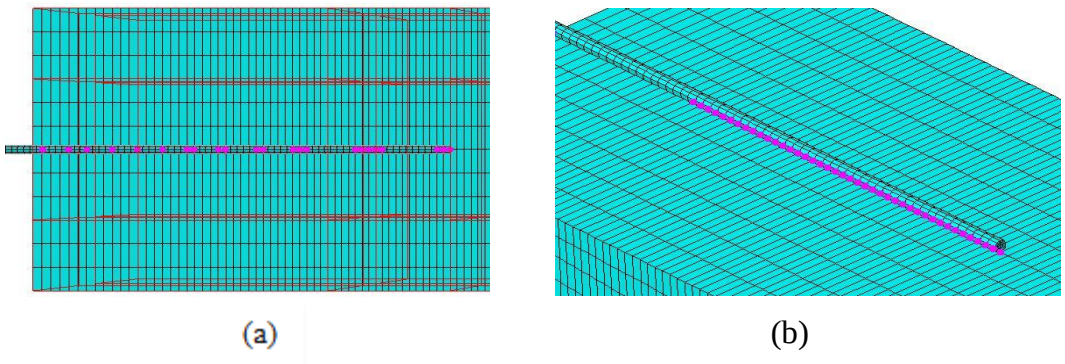

Figure 2.3: Illustration of an imperfect contact between the fork and the fiber, (a) denotes random node merging (imperfect contact), (b) shows that the nodes at the tine end have not been merged (imperfect contact 1)

CHAPTER 3: MATERIAL PARAMETERS

3.1 Material Modeling of Fork

As discussed before, the tuning fork is made up of quartz. The chemical formula for quartz is SiO_2 with the structure formed from chains of Si-O bonds. Quartz shows a trigonal crystal symmetry [20] and hence its material properties are direction dependent. The general constitutive equation of stress and strain for a trigonal crystal in Cartesian coordinate system is given by [20],

$$\begin{bmatrix} \sigma_1 \\ \sigma_2 \\ \sigma_3 \\ \sigma_4 \\ \sigma_5 \\ \sigma_6 \end{bmatrix} = \begin{bmatrix} C_{11} & C_{12} & C_{13} & C_{14} & 0 & 0 \\ C_{12} & C_{22} & C_{23} & C_{24} & 0 & 0 \\ C_{13} & C_{23} & C_{33} & 0 & 0 & 0 \\ C_{14} & C_{24} & 0 & C_{44} & 0 & 0 \\ 0 & 0 & 0 & 0 & C_{55} & C_{56} \\ 0 & 0 & 0 & 0 & C_{56} & C_{66} \end{bmatrix} \begin{bmatrix} \varepsilon_1 \\ \varepsilon_2 \\ \varepsilon_3 \\ \varepsilon_4 \\ \varepsilon_5 \\ \varepsilon_6 \end{bmatrix} \tag{3.1}$$

Quartz has only six independent elastic constants [16-17]: $C_{11}, C_{12}\ C_{13}, C_{14}, C_{33}$, and C_{44}. The C_{ij} matrix for Quartz is,

$$\left[C_{ij}\right] = \begin{bmatrix} C_{11} & C_{12} & C_{13} & C_{14} & 0 & 0 \\ & C_{11} & C_{13} & -C_{14} & 0 & 0 \\ & & C_{33} & 0 & 0 & 0 \\ & & & C_{44} & 0 & 0 \\ & & & & C_{44} & C_{14} \\ & & & & & \frac{1}{2}(C_{11} - C_{12}) \end{bmatrix} \tag{3.2}$$

After a brief search [20-22], the magnitudes of C_{ij} and density were found and used in the model.

3.2 Material Modeling of Fiber

The fiber in the dynamic analysis should ideally vibrate in its first mode. This necessitates a stiffer material for the fiber. A material such as carbon offers a good option. Apart from carbon, other materials such as tungsten, glass, etc. are also employed to manufacture the fibers with different diameters. The carbon fibers of the type 'C005722' produced by 'Goodfellow Corporation, USA' have been used throughout this project. The material characteristics are extracted from their catalogue [23].

3.3 Material Modeling of Glue

Correct selection of the glue, used to attach the fiber on the upper tine of the fork, is critical for a proper functioning of the system. Addition of glue would alter the dynamics of the system and affect the frequency. Furthermore, it is also observed that aged probes, the ones which have been exposed to air for a longer duration, are turned reddish because of the oxidation. Although not in significant magnitude, but aged probes oscillated with differing amplitudes than their non-aged probes counterpart. Thus, using glues with a faster curing time is advantageous. A Norland Optical Adhesive (NOA-61) [23] from 'Norland Products, Inc.' is used to bond the two parts. It is a transparent glue which settles under an ultraviolet light. Some of the salient features of the NOA are:

1) Significantly faster curing time.
2) Typical operations such as premixing or curing using heat, etc. are not required.
3) Slightly flexible, offers good solvent resistance, and is transparent in nature.
4) Good operating temperature range of -150°C to 125°C.
5) Used for bonding lenses, prisms and mirrors for military, aerospace and commercial optics.

Table 3.1: Typical properties of NOA 61 [24]

Density	1231 kg/m^3
Young's Modulus	1034.21 MPa
Tensile strength	20.68 MPa
Elongation at failure	38%

The probes are operating in resonating conditions. No debonding has been observed. Therefore, only elastic properties of the materials are considered.

CHAPTER 4: FINITE ELEMENT MODEL

4.1 Geometry Meshing

After modeling the geometry in Abaqus, finite element analysis of the system is carried out. The most time consuming aspect of preprocessing is part meshing. The industrial part geometries are intricate with many complex contours. Many times, stresses are generated in complex areas. Hence, it is necessary to correctly capture all of the geometries. Owing to this need, some softwares devoted only for the meshing needs, such as Hypermesh, ANSA, etc., have been developed. However, because of the simplicity in the geometry, meshing of the model is also accomplished in Abaqus. From a wide array of available elements, eight noded brick elements have been used both for the fork and fiber. Specifically, the three-dimensional continuum linear elements with reduced integration as denoted by 'C3D8R' in Abaqus/Explicit are exercised. Abaqus chooses reduced integration type by default. It has been found to be computationally inexpensive.

There could broadly be two categories of the fork meshing: the one in which the natural frequencies of the fork are extracted, and the second involving modal as well as dynamic analysis of the probe. A uniform mesh pattern is maintained when the natural frequencies of just the fork are extracted.

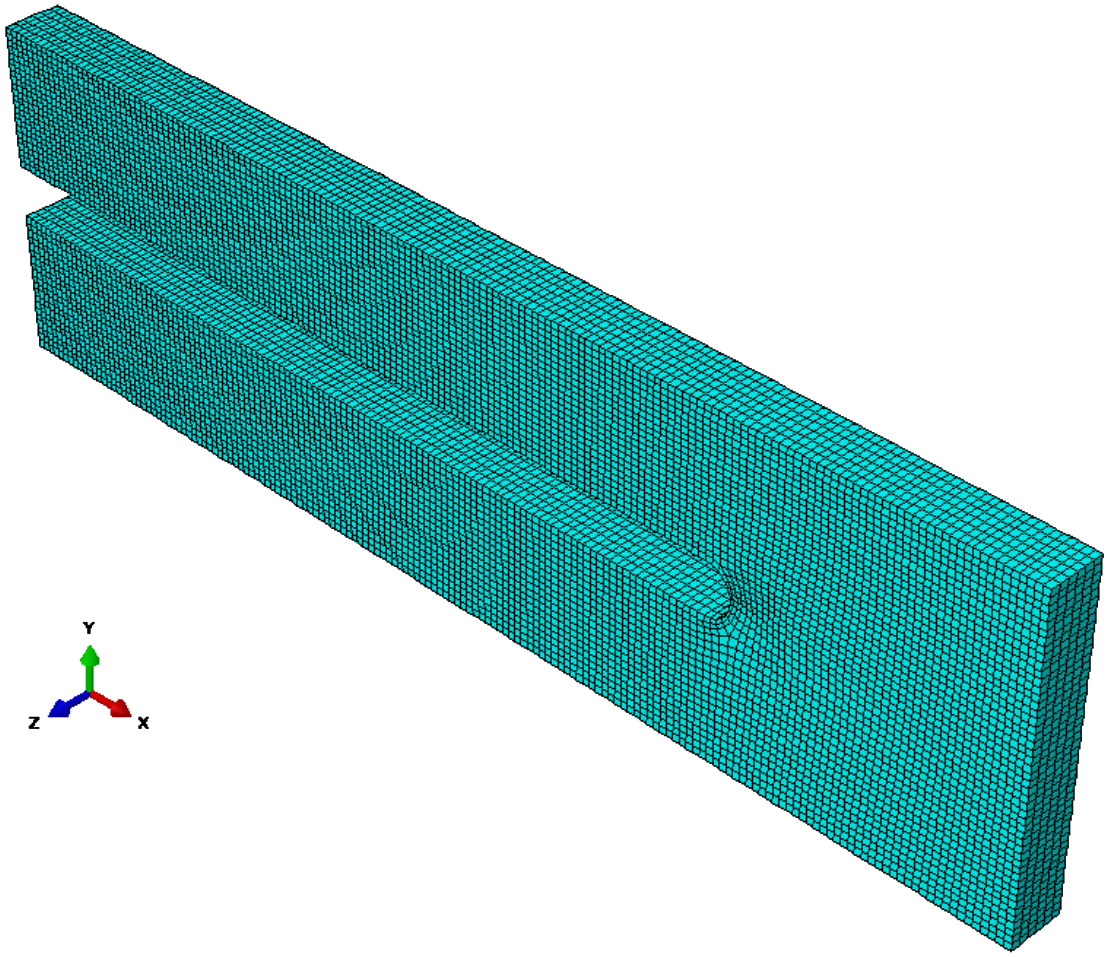

Figure 4.1: Meshing of the fork for its modal analysis

As can be seen in the figure 4.1, the fork is uniformly meshed with a global size of 0.04 mm. Abaqus also provides different type of meshing techniques depending upon the type of element selected. For example, for a hex element, there are certain categories such as free, sweep, structured, etc. Then, there is a meshing algorithm for the overall flow of mesh. The meshing experience showed that ‘sweep’ type of technique coupled with ‘Medial axis’ algorithm and a minimum mesh transition yielded the best possible mesh. Largely, a good mesh pattern was observed for this particular combination and has been employed throughout the project.

For an assembly of the probe, the fiber has been meshed with an element size of 0.005 mm, which is smaller in comparison with that of the fork. At the same time, it is desired to connect the nodes of the respective parts. Reducing the global element size of the fork will result in unnecessary increase in the number of nodes affecting the computational cost. Biased meshing is thus exploited enabling a localized finer mesh at the area of interest with larger elements at other areas. To achieve this, the geometry of the fork is suitably partitioned.

Figure 4.2.a below shows the fork partition. A size of 0.005 mm is maintained along x-direction of the area highlighted in red. Both the tines are partitioned to achieve a symmetry. Figure 4.2.b illustrates the perfect connectivity achieved between the fork and fiber. All of the corresponding nodes are merged with a tolerance of 1×10^{-5} mm.

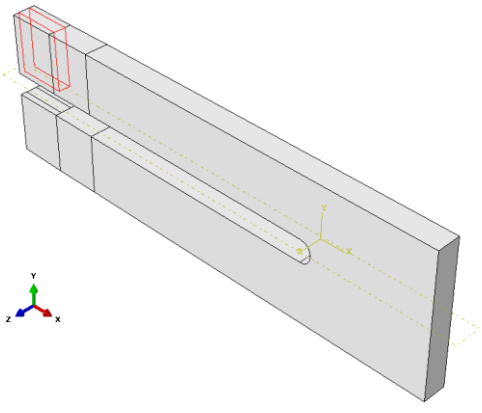

Figure 4.2.a: Fork partition

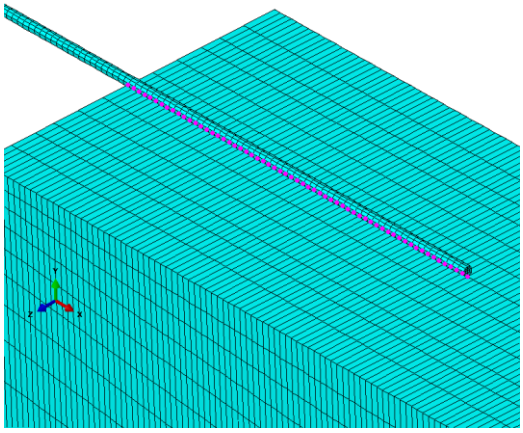

Figure4.2.b: Fork and fiber connectivity

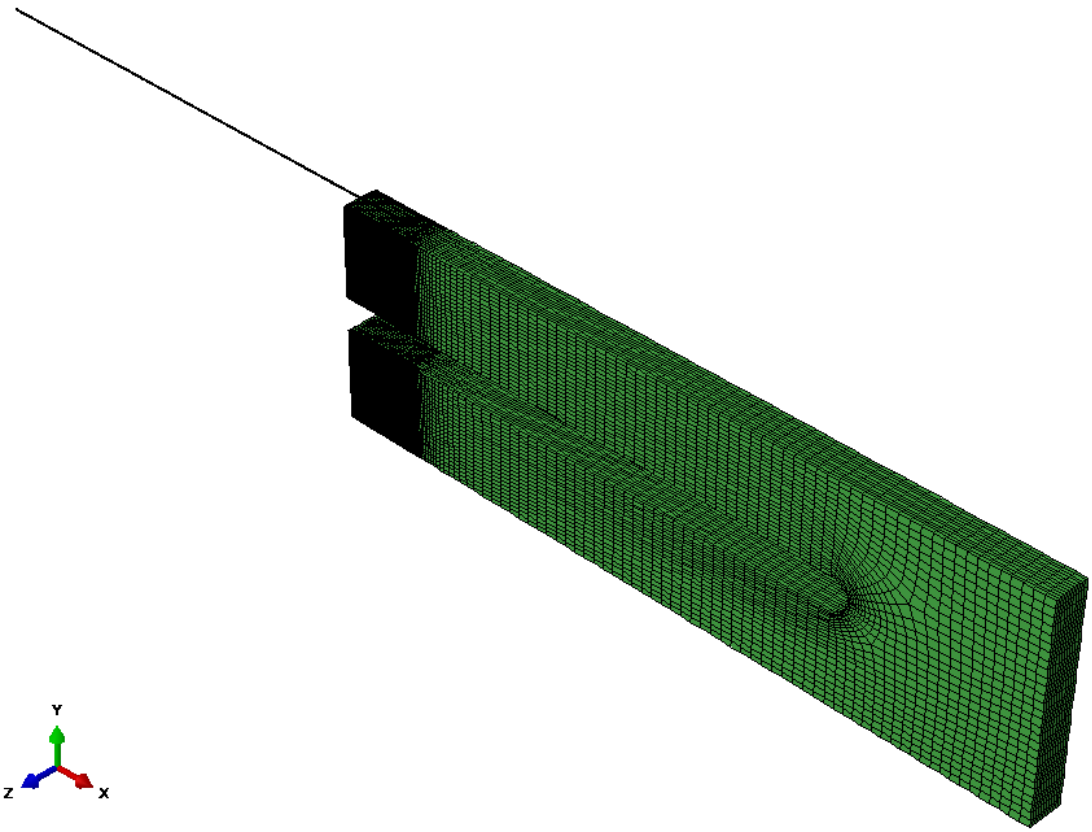

Figure 4.3: Fork and fiber meshed assembly

Figure 4.3 above shows the final meshed assembly system. Use of partition not only helps connect the nodes of the fork with the respective nodes of the fiber, but also allows a smoother transition in the element size.

4.2 Boundary Conditions

Both for the modal and dynamic analysis, end of the fork is fixed. An external load in the form of a sinusoidal wave ($F=A\sin\omega t$, N) has been applied in the dynamic simulation. Duration of the load is 3.906 milliseconds, which is 125 times the period of excitation frequency. Amplitude of the load is a body force (force per unit volume) with a random value of 34 $\mu N/mm^3$. Figures 4.4 and 4.5 denote the boundary conditions for mode 3 and mode 4 type loadings respectively. It can be seen that in mode 3 type loading, both the tines

are allowed to move in the same direction, while mode 4 type loading, the tines move in the opposite directions.

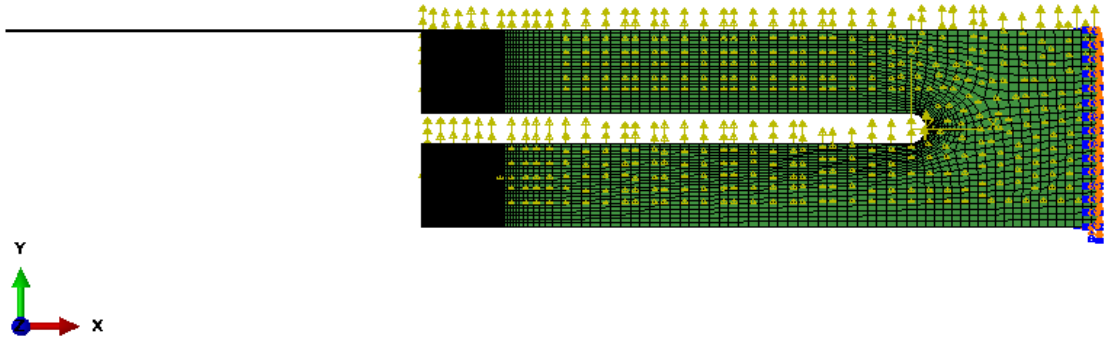

Figure 4.4: Boundary conditions for the dynamic simulation with mode 3 loading

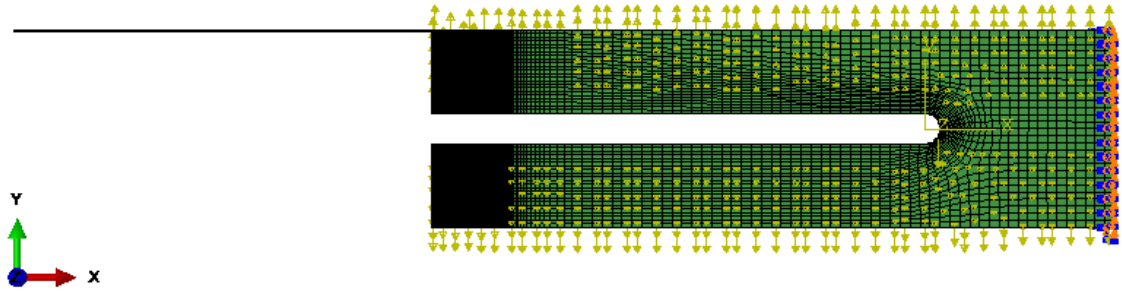

Figure 4.5: Boundary conditions for the dynamic simulation with mode 4 loading

4.3 FEM Solving

The finite element solving procedure in the project could be categorized into two groups: 1) Modal analysis, and 2) Dynamic analysis.

4.3.1 Modal Analysis

In this procedure natural frequencies of the model are extracted. Numerous solving algorithms in FEM are available for an eigen frequency extraction. Jeffrey K. Bennighof et al [25] used an automated multilevel substructuring (AMLS) method to get the natural frequencies of the system. Similarly there are other methods such as Lanczos, Subspace iteration, etc. [26-28], and are found in Abaqus library. The most widely used algorithm is Lanczos method as it is computationally inexpensive [29-30]. Lanczos algorithm is thus employed to calculate Eigen modes of both the fork and the probe.

4.3.2 Dynamic Analysis

The dynamic analysis of the system is accomplished through Abaqus/Explicit version 6.11. As mentioned before, simulation has been run for 3.906 milliseconds. It may be noted that Abaqus/Standard could also have been utilized in the project. However, explicit technique is used to work out the problem owing to its general popularity to tackle non-linearity, contact modeling, etc.

In Abaqus/Explicit, central difference rule is used to calculate instantaneous kinematic condition from the kinematic condition in previous step [31]. Thus,

$$\ddot{u}_{(t)} = (M^{-1})(P - I)_t \tag{4.1}$$

$$\dot{u}_{(t+\frac{\Delta t}{2})} = \dot{u}_{(t-\frac{\Delta t}{2})} + \frac{(\Delta t_{(t+\Delta t)} + \Delta t_{(t)})}{2} \ddot{u}_{(t)} \tag{4.2}$$

$$u_{(t+\Delta t)} = u_{(t)} + \Delta t_{(t+\Delta t)} \dot{u}_{(t+\frac{\Delta t}{2})} \tag{4.3}$$

where *M, P, I, u* are nodal mass, instantaneous externally applied force, internal element force, and displacement matrices respectively. Correspondingly, $\ddot{u}$, and $\dot{u}$ are instantaneous acceleration and velocity matrices. Hence, it can be seen that balance of dynamic equilibrium at the beginning of the increment would yield acceleration, from which instantaneous velocity and displacement can be determined. Also, size of increment would decide the computational time and accuracy of the results. Lesser the increment, better is the accuracy, at the cost of computational time. The stable time increment in an explicit analysis is calculated using,

$$\Delta t = \frac{L_{\min}}{C_d} \tag{4.4}$$

where L_{min} is the length of a smallest element in the meshed part, and C_d is a parameter referred to as 'dilatational wave speed' and its values are material dependent. In general, the value of dilatational wave speed in 3-D continuum for a linear isotropic material is given by [32-33],

$$C_d = \sqrt{\frac{E(1-\nu)}{(1+\nu)(1-2\nu)\rho}} \tag{4.5}$$

Hence, for a given material, the stable time increment is governed by length of the smallest element in mesh. If the mesh is finer, it will be small. In most cases, a finer mesh in a complex region is desired. But because of such a particular portion or a bad element in the assembly, stable time increment for the whole model is affected. Such an inconvenience can be eliminated by managing the degree of dilatation wave speed. It can be seen from equations 4.4 and 4.5 that an increase in the density can help improve the stable time increment. This is achieved in finite element methods by artificially adding density to the model through a "mass scaling". It can be ensured in Abaqus by manually

entering a factor value. One has to be judicious selecting the value as entering a larger value would alter the physics of the problem and yielding inaccurate results. Typically, the results hold well, if the ratio of kinetic to internal energy of the system is less than 10% [30]. In the project, owing to the minute size of the fiber, its element size is comparatively smaller resulting in overall tiny stable time increment. After a considerable simulations, a mass scaling factor of 1.1 was specified to the fiber elements with a minimal change in accuracy. The ratio of kinetic energy to internal energy for this factor value was approximately 1 throughout the simulation.

4.3.2.1 Bulk Viscosity Parameters

The probe experiments have been conducted in a temperature controlled room. The resistance offered to the tip motion is in the form of air only, which is negligible. The damping in the finite element model is introduced through bulk viscosity parameters. These are especially useful in the high speed occurring simulations. Abaqus/Explicit allows to implement them through Linear and Quadratic bulk viscosity factors. Linear factor is used for ‘truncation frequency damping’, i.e. it will damp out any unnecessarily excessive element frequency to have a stability in the model. The quadratic scale factor is applied only in solid continuum elements and is useful for compressive loading only. The default values of 0.06 and 1.2 for linear and quadratic scaling respectively have been used throughout the thesis work [31].

4.3.2.2 Contact Analysis

When the glue is modeled in the simulation, there are two contacting interactions: upper layer of glue is in contact with the fiber, while the lower layer touches the fork. The interactions among different surfaces is defined in Abaqus using contact formulation. A

general contact algorithm is employed in the thesis, which is defined in Abaqus using ‘master’ and ‘slave’ surfaces. A master surface is allowed to penetrate into the slave, but the reverse is generally not true [34]. Slave surfaces have softer material properties and/or a finer mesh. In this case, the glue can neither penetrate into the fork nor fiber and hence, has ultimately been treated as a slave surface throughout the contact analyses.

There are two contact discretization available in Abaqus/Explicit library. One provides finite sliding surface-to-surface algorithm, while other employs node-to-surface contact discretization. The finite sliding surface-to-surface discretization procedure is used in a general contact algorithm. It has been observed that the node-to-surface discretization generates uneven distribution of pressure across the surface, whereas pressure is uniformly spread in the model when surface-to-surface algorithm is used [31]. Due to this reason, surface-to-surface contact method is exercised in the thesis. Figure 4.6 depicts a close view of the mesh being employed for a contact analysis model.

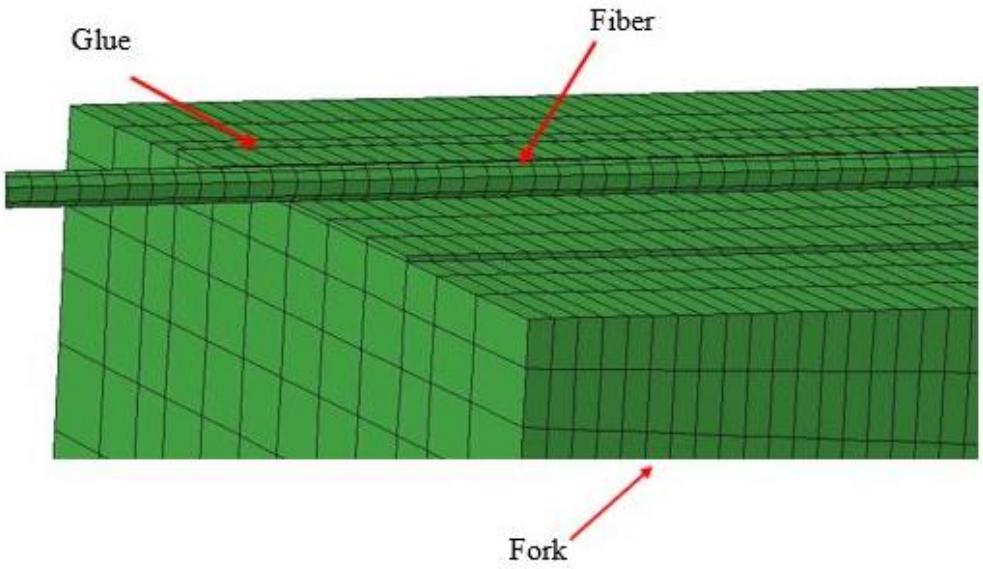

Figure 4.6: Mesh for contact analysis

CHAPTER 5: RESULTS AND PARAMETRIC STUDIES FOR MODE 3 LOADING

5.1 Modal Analysis

In this section, results of modal analyses of the fork and the probe are discussed.

5.1.1 Modal Analysis of Fork

The thesis work was started with a simple study of extracting natural frequencies of the fork. It is worth to mention that symmetric and anti-symmetric modes of vibration hold significance in the research. In the symmetric mode, both tines of the fork move in the same direction perpendicular to their length, while in the anti-symmetric mode, the tines move in an opposite direction. Both the modes have been depicted in the figure 5.1. The anti-symmetric mode is important because of its unique motion due to which net momentum in the system is nullified. This helps giving a good grip to a user when the forks with a handle at its end are held. In this case, an electrode coating is so made on the fork that anti-symmetric mode gets excited in a forced vibration. Nevertheless, both modes are studied in the dynamic simulations.

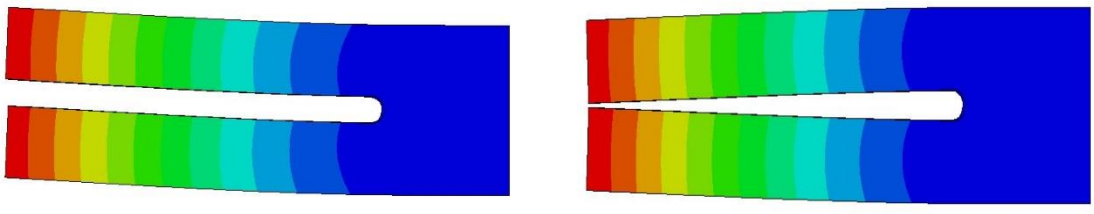

(a) (b)

Figure 5.1 (a) and (b): Symmetric and anti-symmetric modes of the fork respectively

Natural frequencies of 33175 Hz and 34537 Hz are obtained for symmetric and anti-symmetric modes respectively and used later in the dynamic simulations.

5.1.2 Modal Analysis of Probe

After calculating the natural frequencies pf the fork, the next task was to compute such values for the probe. Modal analysis for different lengths of probes has been carried out. It is observed that change of length alters both the eigen value and the eigen mode. Some of the eigen mode and eigen frequencies are listed in table 5.1. The frequencies marked with '*' are the frequencies of interest. They represent anti-symmetric movement of the tines. Note the close spacing of frequencies. Also, the eigen mode has been pushed from 11 to 13 with increase in length. The aim of this analysis is to observe the pattern of natural frequencies with varying length of the fiber.

Table 5.1: Natural frequencies of probes with varying fiber lengths

Fiber Length (mm)	Eigen Mode	Eigen Frequency (Hz)
3.20	10	33187
	11	*34560
	12	36854
3.25	10	33187
	11	*34558
	12	35621
3.30	10	33185
	11	34418
	12	*34587
	13	35072
3.35	10	33167
	11	33343
	12	33938
	13	*34565
3.40	10	32255
	11	32856
	12	33191
	13	*34563
3.50	10	30277
	11	30844
	12	33189
	13	*34562
3.65	10	27633
	11	28156
	12	33188
	13	*34561
3.80	10	25320
	11	25804
	12	33188
	13	*34561

5.2 Dynamic Analysis

All the results of the dynamic simulations discussed in this chapter represent mode 3 (symmetric mode) type loading of the fork. The dynamic simulation is started with a 3.50 mm fiber length and frequency of 32768 Hz, which is a theoretical natural frequency of QTFs. A typical plot for the fiber tip displacement in y-direction as a function of time is shown in figure 5.2: The tip continues to stay in transient condition for a while after which it almost stabilizes. The presence of 'beats', which represent interference of two different frequencies, shows that there are two dominant modes in the transient region. It can also be seen from the trace that one of the frequencies has been damped out.

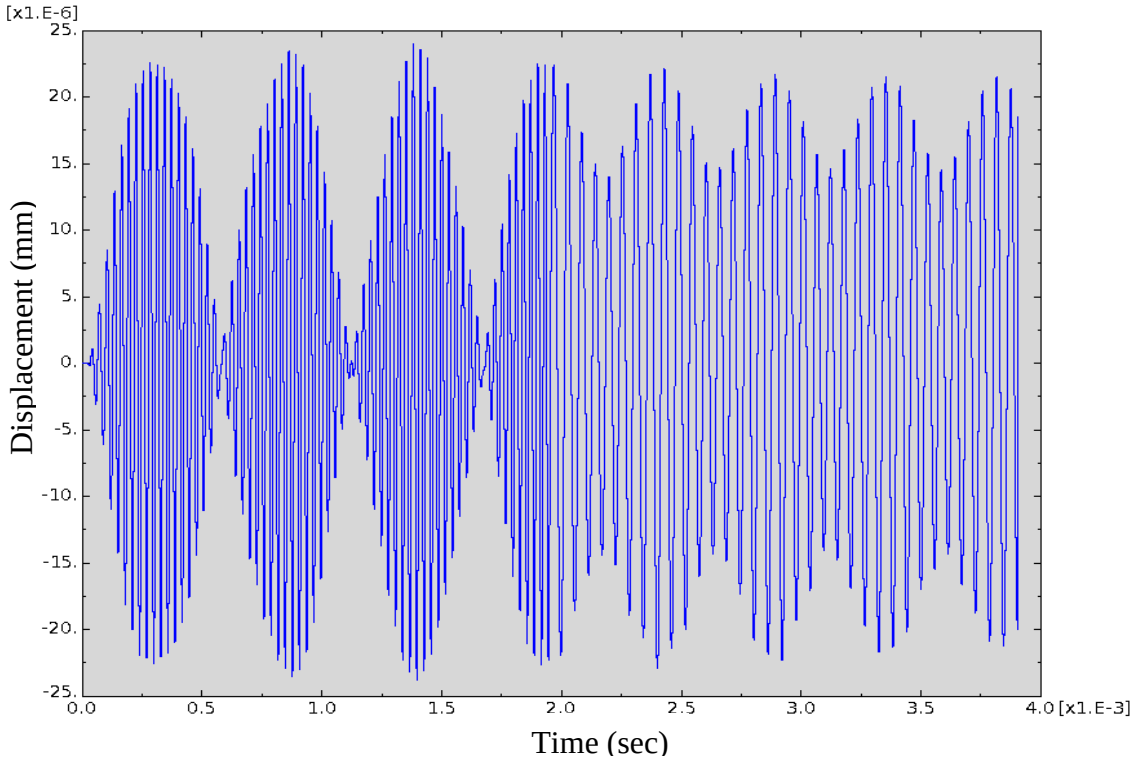

Figure 5.2: Graph of tip displacement with time

5.2.1 Mesh Sensitivity Analysis

The FE model has been tested for the mesh sensitivity to check if the results are converged. The assembly is re-meshed to achieve a 25% refinement in element density. Displacement at the tip is used for the solution convergence test. Maximum element size in y-direction at the tine end in a biased mesh region is 0.079 mm, while for a refined mesh it is 0.059 mm. Along the tine length in x-direction, the nominal size is 0.080 mm. In case of a refined mesh, the mesh size is 0.070 mm. The number of elements along the thickness of tine are arbitrarily increased. The total number of elements for non-refined and refined mesh thus stand at 84170 and 104784 respectively.

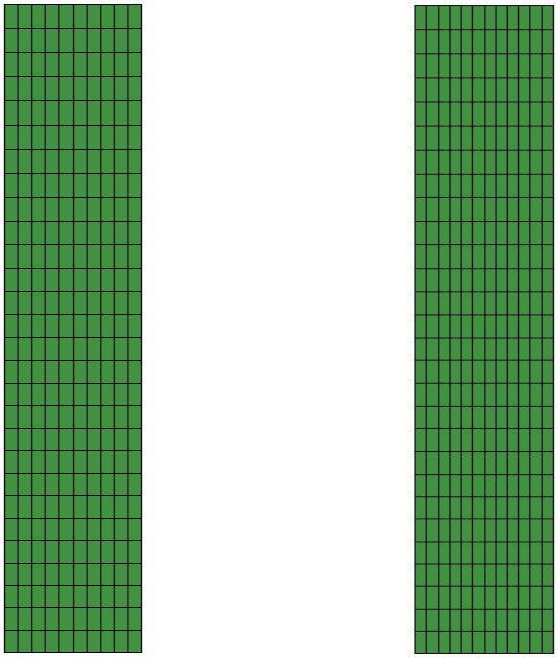

(a) (b)

Figure 5.3 Side view of (a) coarse mesh, and (b) refined mesh, for the assembly

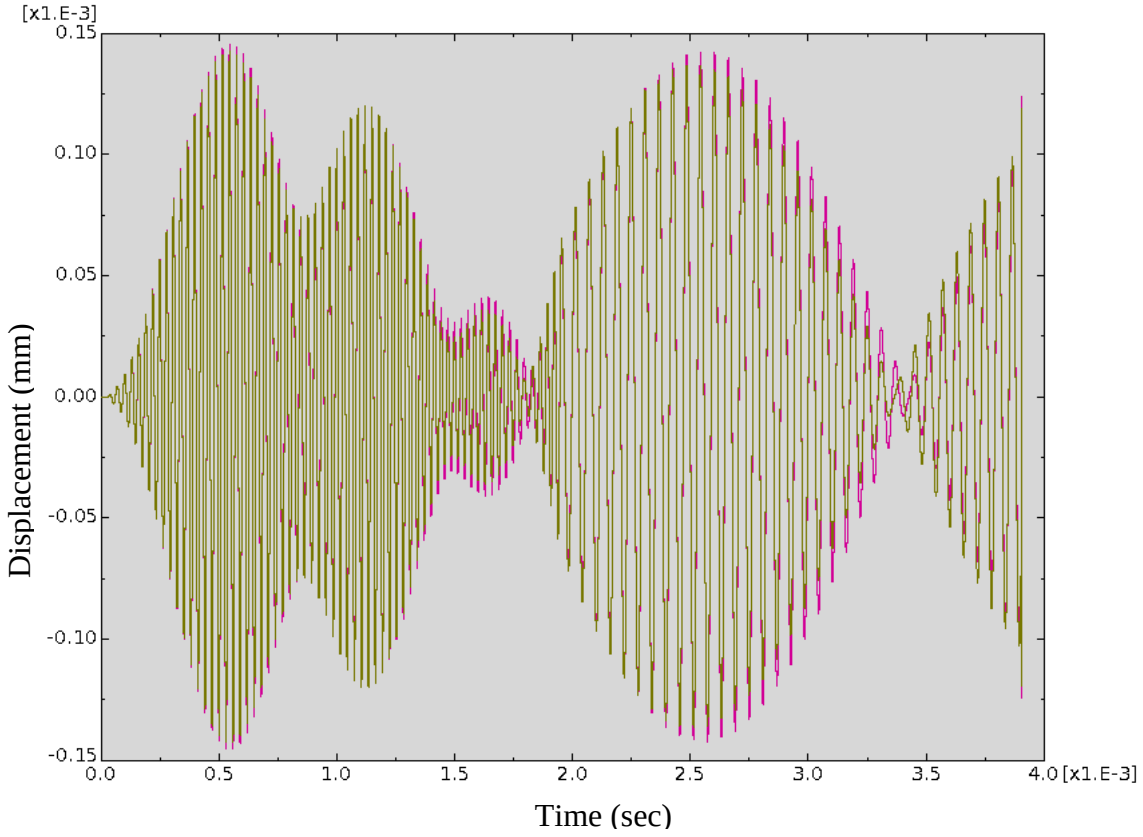

Figure 5.4: Plot of fiber tip displacement against time for coarse and refined mesh

The tip displacement curve for coarse and refined mesh is shown in figure 5.4. The plot obtained is for fiber length of 3.35 mm and the forcing frequency being 32768 Hz. It can be seen that the tip path matches for both the curves. It is thus safe to assume that numerical solution for the dynamic analysis has been converged.

5.3 Parametric Studies

After initial results of the tip displacement, the numerical model has been expanded to study the effects of different parameters on the tip displacement. As mentioned earlier, three potentially influencing factors, namely length of fiber, loading frequency, and placement of the fiber on the fork, are considered. Their effects are discussed below:

5.3.1 Length of Fiber

To begin with, fiber lengths from 3.20 mm to 3.80 mm with a spacing of 0.15 mm have been considered in the study. Because of the relatively higher value of the tip displacement at fiber length of 3.35 mm, the scale is further split up at 3.20 mm, and with an interval of 0.05 mm, tip displacement for fiber lengths of 3.25, 3.30, and 3.40 mm is also probed. The tip displacement for each of these fiber lengths is enlisted in table 5.2.

It is seen that fiber tip displacement is maximum at the fiber length of 3.30 mm. The graph for the tip displacement against fiber length (figure 5.5) thus shows a peak at 3.30 mm. For the probes with fiber length 3.50 mm onwards, there are no significant tip displacements.

Table 5.2: Tip displacement in y-direction for different fiber lengths: mode 3 loading

Fiber Length (mm)	Tip Displacement (μm)
3.20	0.040
3.25	0.100
3.30	0.570
3.35	0.140
3.40	0.115
3.50	0.0225
3.65	0.0150
3.80	0.008

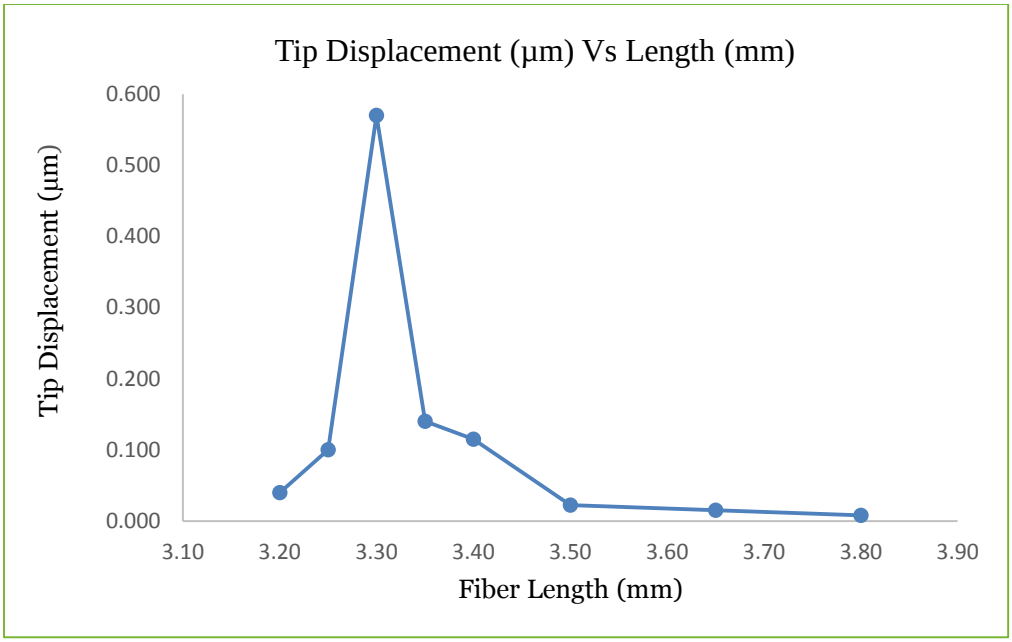

Figure 5.5: Graph for the tip displacement as a function of fiber length

Another point to note is four nodes are spotted along the fiber length, which matches with the laboratory observations. A typical photograph taken from the experimental work is shown below. Also shown are figures 5.7 (a) and (b) obtained from Abaqus that illustrate the vector displacements at an instantaneous time along the points on the fibers of 3.30 mm and 3.50 mm in length.

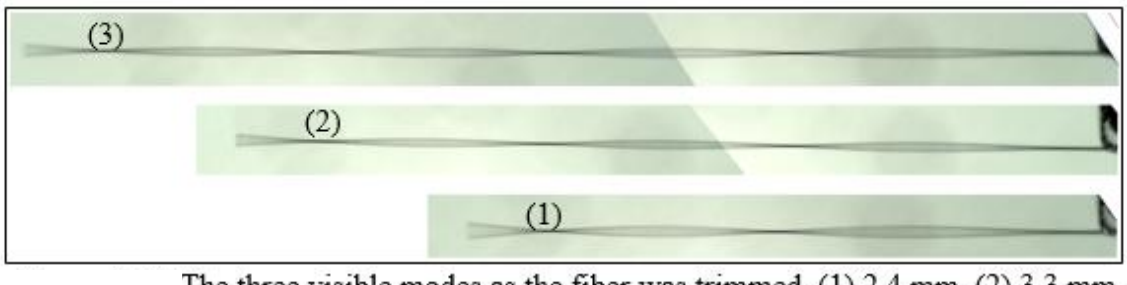

The three visible modes as the fiber was trimmed. (1) 2.4 mm, (2) 3.3 mm, (3) 4.3 mm. These images are only approximately to scale relative to one another.

Figure 5.6: Picture depicting nodes observed in the experiment, taken from [19]

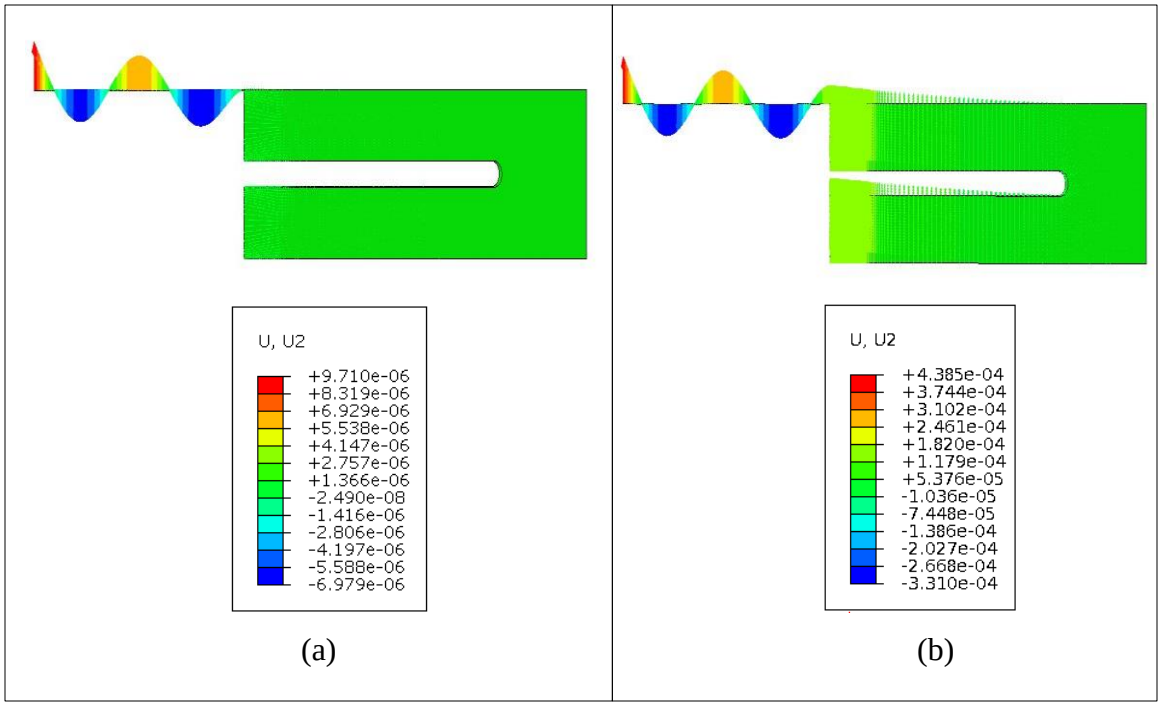

Figure 5.7: Vector displacement of fibers, (a) 3.30 mm, and (b) 3.50 mm at 2.36 milliseconds, in millimeters

For shorter lengths of fiber, less number of modes would be obtained. However, the fiber length needs to be sufficiently large enough. Otherwise, when submerged in the medium, the slurry particles may jump on the fork tine affecting the dynamics of the process completely. With longer spans of fiber, more number of nodes would be developed even for a material as stiff as carbon at the given frequency of excitation.

Because maximum tip displacement is observed at 3.30 mm length of fiber, it has been selected later for executing further analyses.

5.3.2 Effect of Frequency

A frequency swipe analysis is performed to study the effect of forcing frequency on the tip displacement. This is achieved using an ‘explicit run’ being simulated with different exciting frequencies. A range of 32000 Hz to 35000 Hz with an interval spacing of 1000 Hz is selected for a 3.35 mm fiber length probe. A similar analysis is also carried out for a probe with 3.30 mm fiber, with close intervals of 500 Hz. The results are plotted in figures 5.8 and 5.9 respectively.

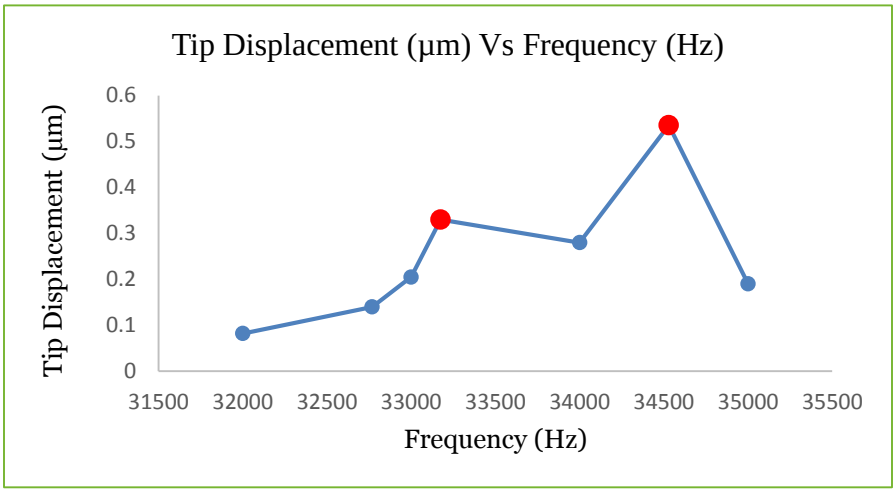

Figure 5.8: Plot illustration of tip displacement variation with frequency

Table 5.3: Tip displacements for a probe of 3.35 mm fiber length at different frequencies

Fiber Length: 3.35 mm	
Frequency (Hz)	Tip Displacement (µm)
32000	0.082
32768	0.140
33000	0.205
33175	0.330
34000	0.280
34530	0.535
35000	0.190

The red colored points denote resonant frequency points. Understandably, tip exhibits maximum oscillations at resonance. Such a trend is observed for 3.30 fiber too, the results of which are tabulated below:

Table 5.4: Tip displacement for a probe of 3.30 mm fiber length at different frequencies

Fiber Length: 3.30 mm	
Frequency (Hz)	Tip Displacement (μm)
32000	0.300
32500	0.350
32768	0.570
33000	0.450
33175	0.627
33500	0.580
34000	0.937
34100	1.180
34200	1.950
34300	3.150
34400	4.150
34500	4.950
34530	5.000
34600	4.770
35000	1.200

As shown, a maximum tip displacement of 5 microns has been obtained for the fiber length of 3.30 mm, and at the resonating frequency of 34530Hz. A small rise in the displacement is also reported at 33175 Hz.

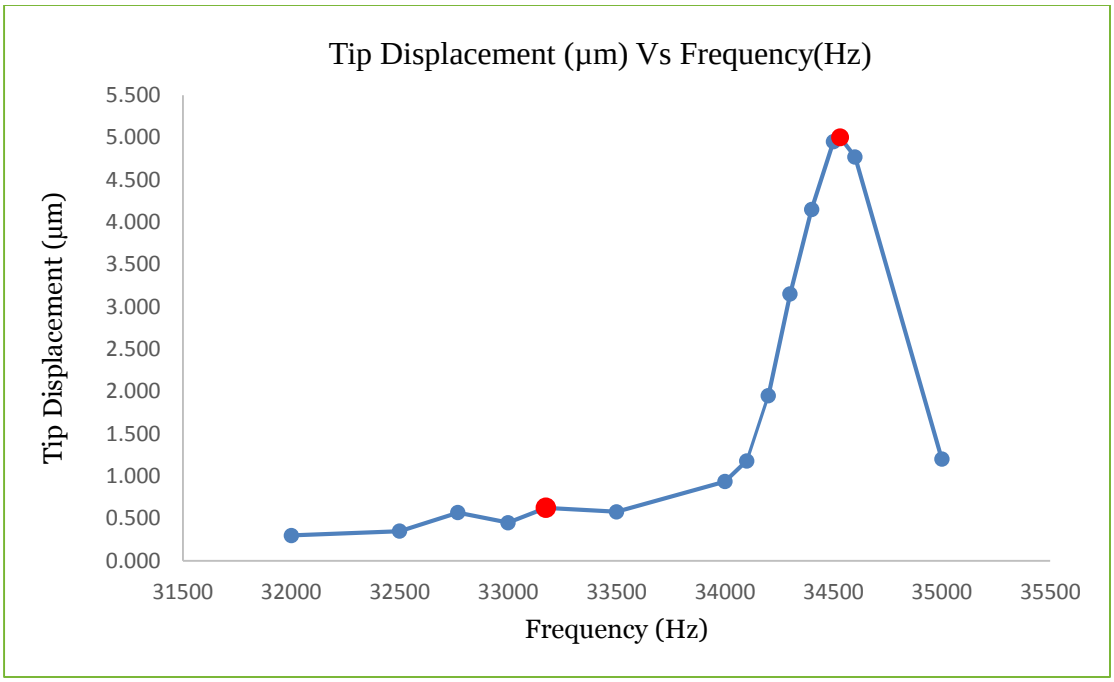

Figure 5.9: Plot illustrating tip displacement variation with frequency

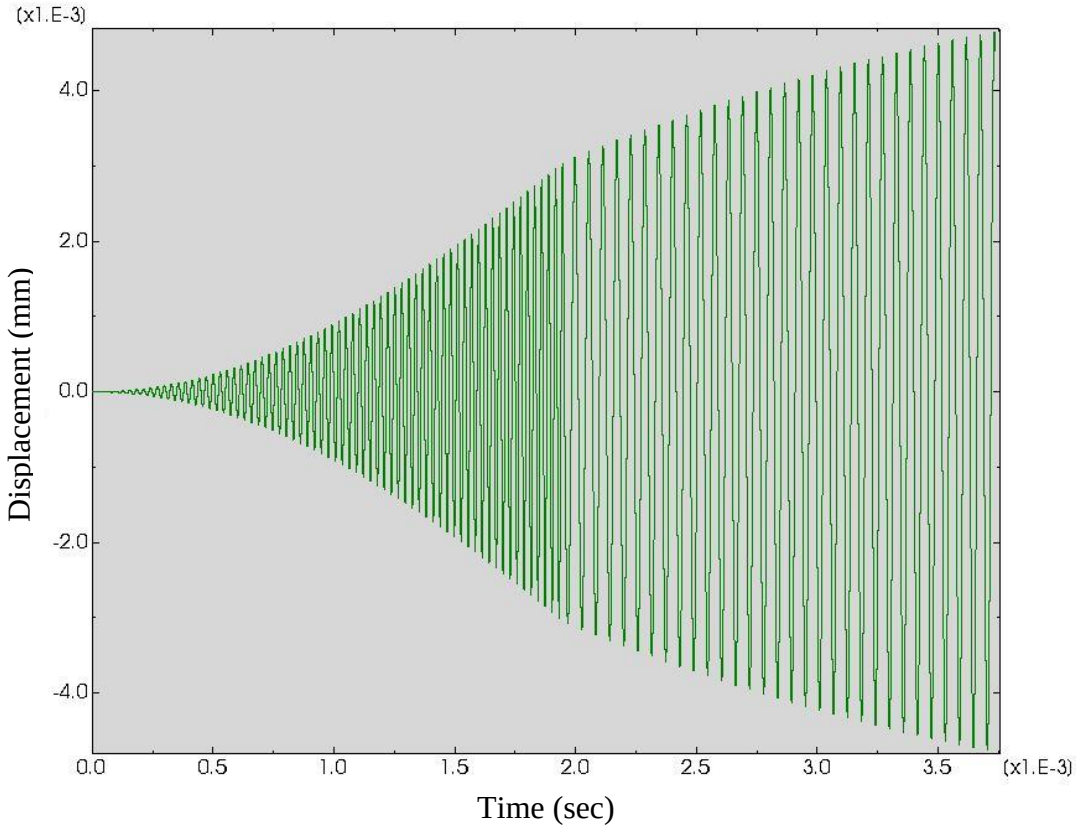

Figure 5.10: Graph of tip displacement with time

Figure 5.10 shows the plot of tip displacement for the probe with 3.3 mm fiber length and simulated at 34530 Hz. It can be again seen that there are two dominant frequencies initially in the transient region (dense lines), while one of the frequencies gets damped out later. Fast Fourier Transform (FFT) in frequency domain is used to determine the values of dominant frequencies exhibited in the model.

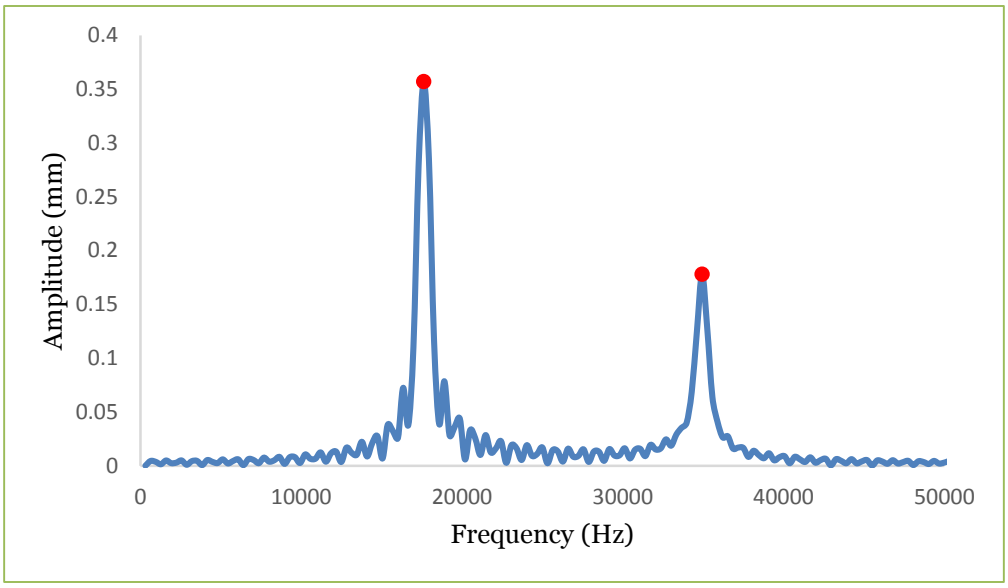

Figure 5.11: Plot of amplitude against frequency

The plot of amplitude against frequency is shown in figure 5.11. It is clear from the figure that two frequencies (shown by red dot) are dominant in the simulations. Their values stand at 34936 Hz and 17628 Hz. The higher frequency of 34936 Hz represents the exciting frequency in the model, while the existence of lower frequency, which is almost half the value of 34936 Hz, shows a sub-harmonic response in the model. This frequency is close to one of the natural frequencies (17576 Hz) of the probe, calculated during the modal analysis. Thus, two modes excite the system in the transient state.

5.3.3 Effect of Misalignment

With the geometry of the probe being too small, it is extremely difficult making a perfectly aligned probe. Even after meticulously making the joints, it is highly likely that the fiber might have a misaligning placement with respect to the fork axis. It is thus imperative to study the effect of misalignment on the fiber tip oscillations. As already mentioned in chapter 2, different modeling scenarios of offset, skew, offset-skew, and imperfect contact geometries are consequently built. Schematic of offset and skew placements are illustrated in figure 5.12. Three offset positions of 0.030, 0.045 and 0.060 mm, and three angular positions of 3°, 5° and 7° with respect to central axis of the upper tine are considered. A perfect node-to-node coonectivity along the line of contact for all of the cases is maintained. A probe with fiber measuring 3.35 mm in length was utilised in the simulation. The results for such a study are presented in table 5.5.

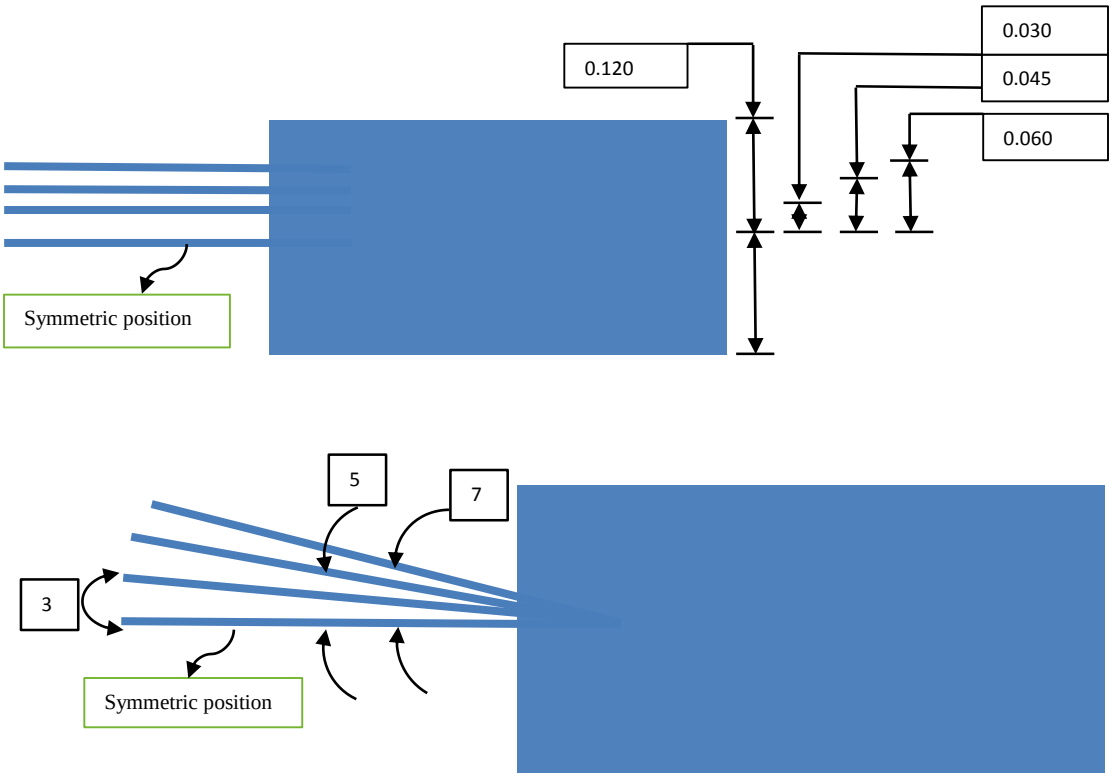

Figure 5.12: Offset and skewed positions of fibers with respect to central axis of the fork tine. Figures are not according to the scale, all the respective dimensions are in mm and degrees

Table 5.5: Values of tip displacements due to (a) offset geometry, and (b) due to angular geometry

Effect of Misalignment Offset Geometry	
Offset Distance (mm)	Tip Displacement (μm)
0.030	0.140
0.045	0.150
0.060	0.140

(a)

Effect of Misalignment Skewed Geometry	
Angular Position	Tip Displacement (μm)
3°	0.140
5°	0.150
7°	0.140

(b)

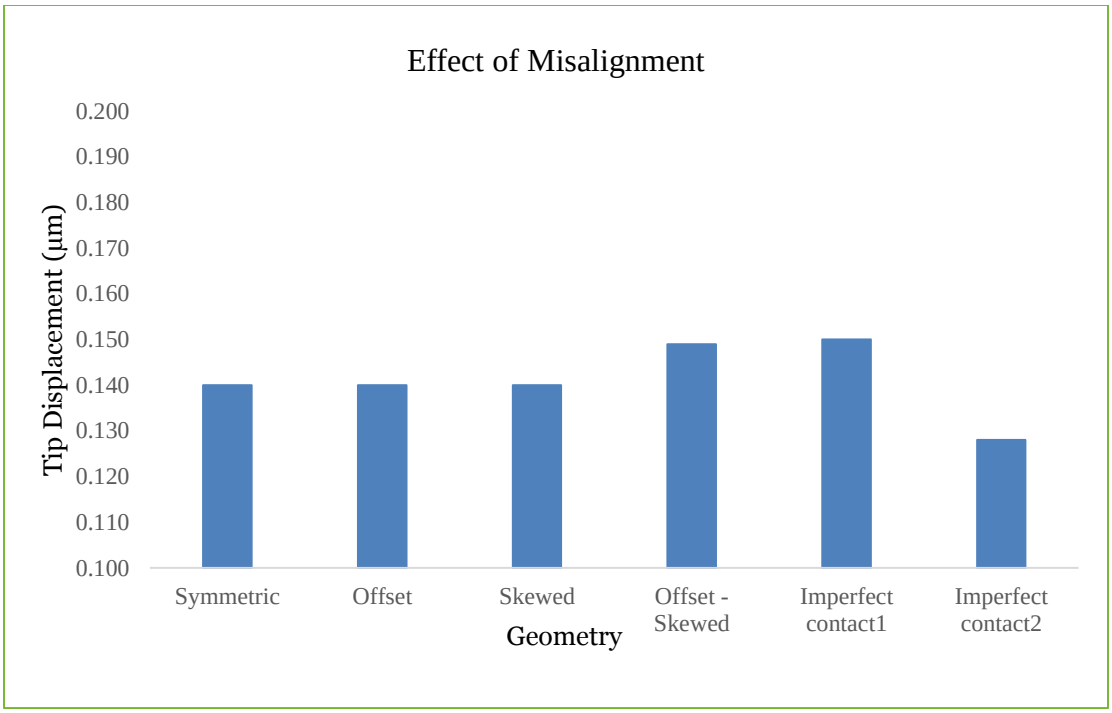

Figure 5.13:A chart summerizing effect of misalignments

The values of both the symmetric and misalignment positions, along with the results for imperfect contact simulations are summerised in the histogram displayed in figure 5.13. It can be seen except for the case of imperfect contacts that misalignments barely affect the tip oscillations. This is also confirmed from the experimental studies, where several probes being oberved under the microscope yielded similar magnitudes of tip displacements.

5.4 Trace of the Fiber Tip

One point to note is the tip also has a motion in z-direction. That means, the motion is not in one plane. The path of the tip, if traced, thus produces a cirular or an elliptical trajectory . The image obtained from the experimental observations of such a trace is shown in figure 5.15. A faint elliptical loop can be seen at the end. A Matlab plot of displacements in y and z directions obtained from Abaqus yielding an elliptical shape in a two dimensional plane is shown in figure 5.14a. A three dimensional plot (figure 5.14b) with time being a

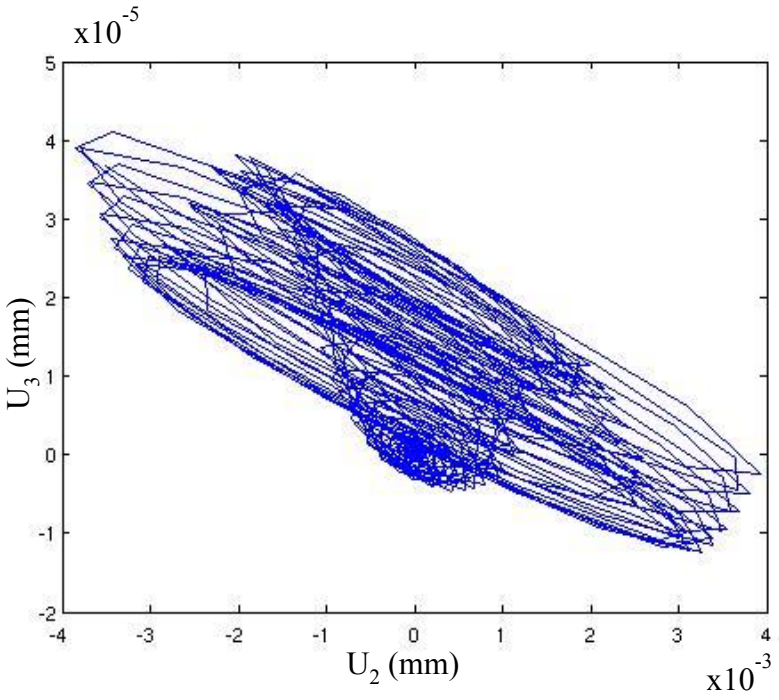

(a)

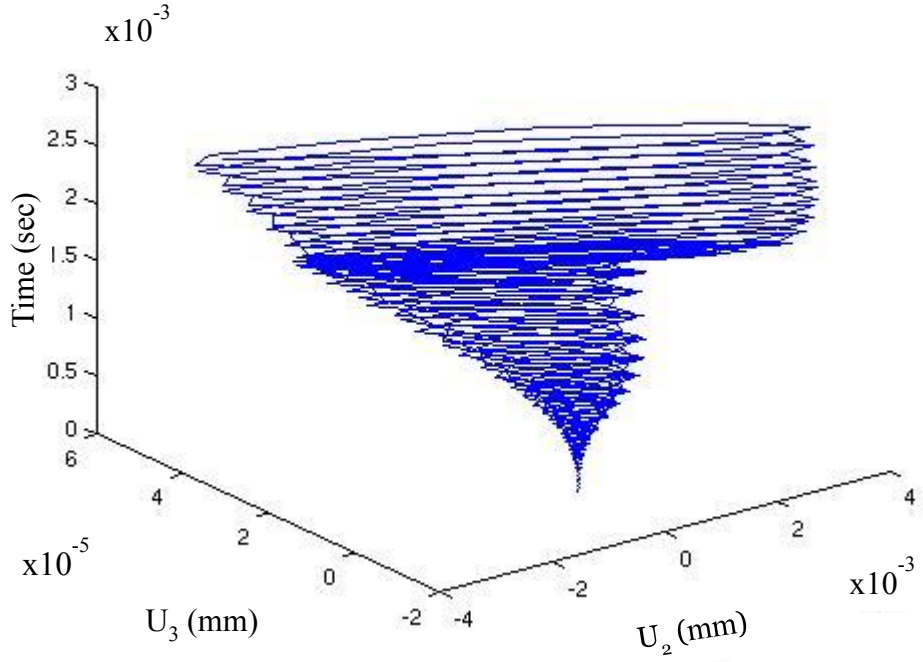

(b)

Figure 5.14 (a), (b): Trace of the fiber tip for symmetric position

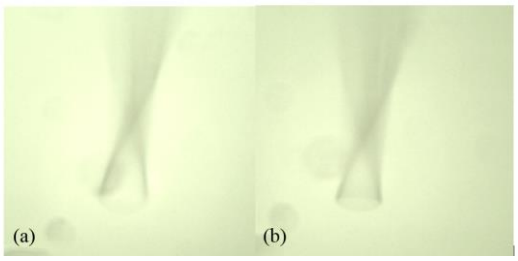

Figure 5.15: Elliptical loop seen at the fiber tip, adopted from [19]

third dimension is also presented. It consists of a number of elliptical loops in time domain. The size of the loop initially grows significantly displaying a transient region, which almost steadies afterwards. Figures 5.16 (a) and (b) also depict such plots for an offset-skew position.

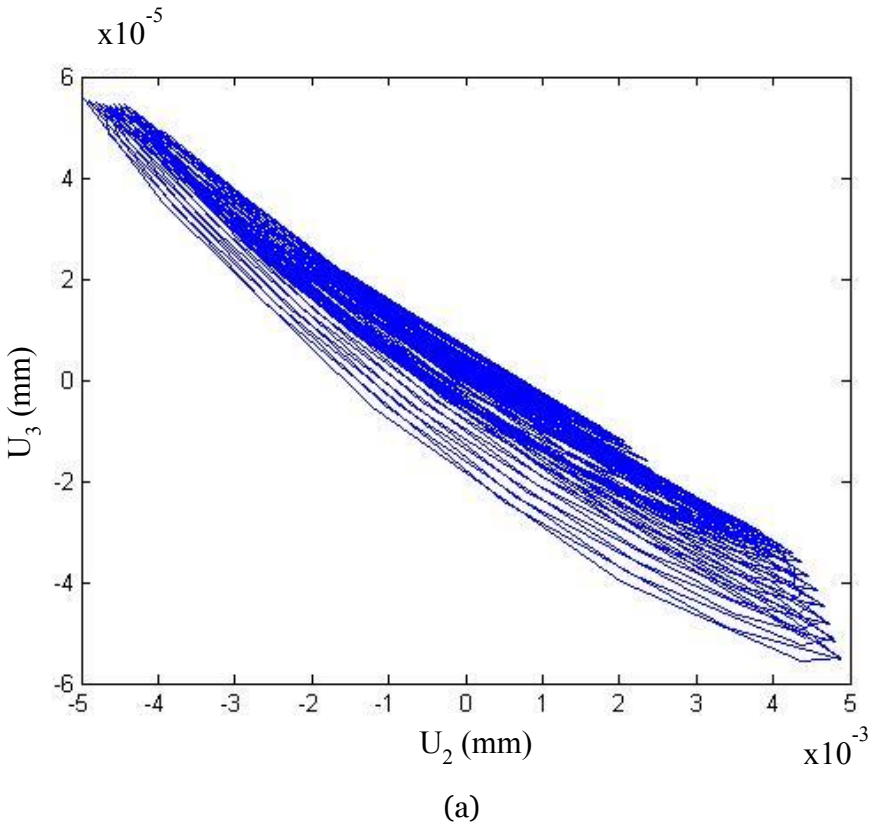

(a)

Figure 5.16 (a): Trace of the fiber tip for offset-skew position

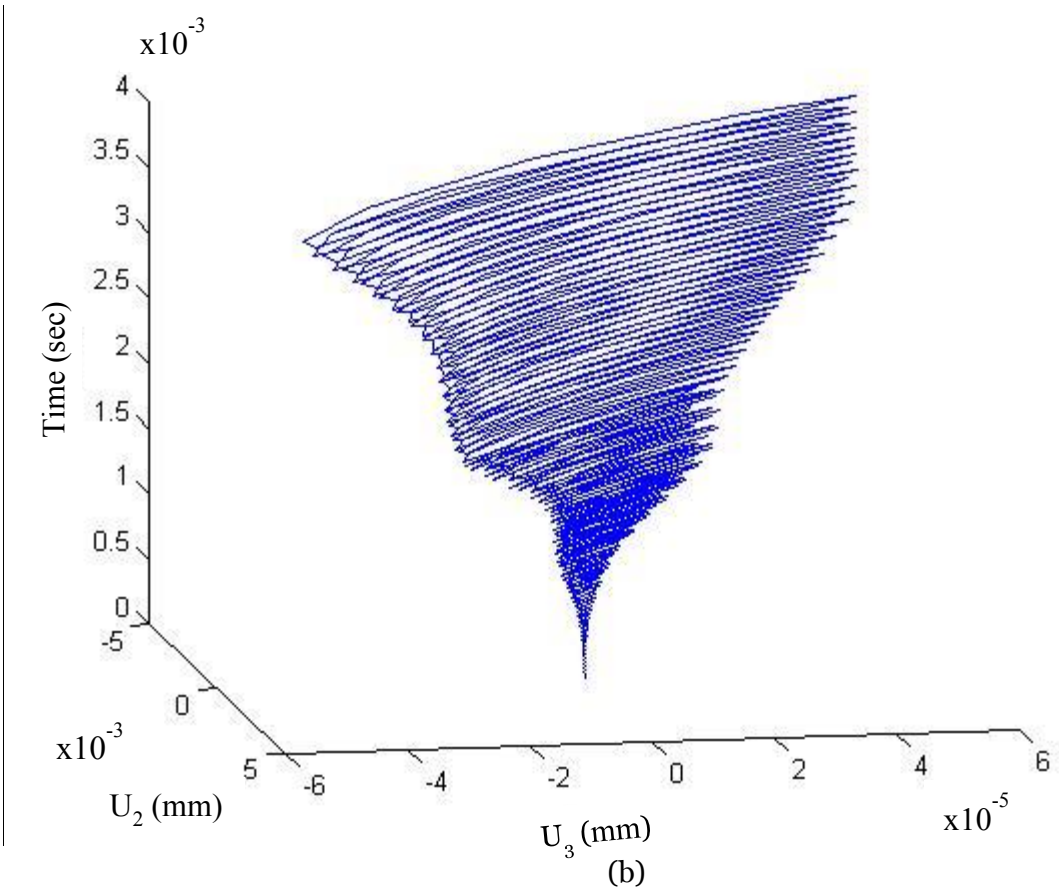

Figure 5.16 (b): Trace of the fiber tip for offset-skew position

5.5 Glue Contact Analysis

After performing parametric studies with the fiber and fork, the probe has been modified to incorporate a glue in the model. As mentioned in chapter 4, contact analyses are performed with 'Norland Optical Adhesive' acting as the glue. Both the step time of 3.906 seconds and boundary conditions in the simulations are the same as the probe without the glue. A frequency swipe analysis is accomplished using the probe of 3.30 mm fiber length. In this case also, the probe is simulated explicitly with the frequency range of 32000 to 35000 Hz. The result table and the graph for the variation of tip displacement with frequency are presented in table 5.6 and figure 5.17 respectively.

Table 5.6: Results of frequency swipe analysis for a glued probe

Glued Probe	
Fiber Length: 3.30 mm	
Frequency (Hz)	Tip Displacement (µm)
32000	0.06
32500	0.08
33000	0.1
33175	0.2
33500	0.19
34000	0.71
34500	1.6
34530	1.6
35000	0.45

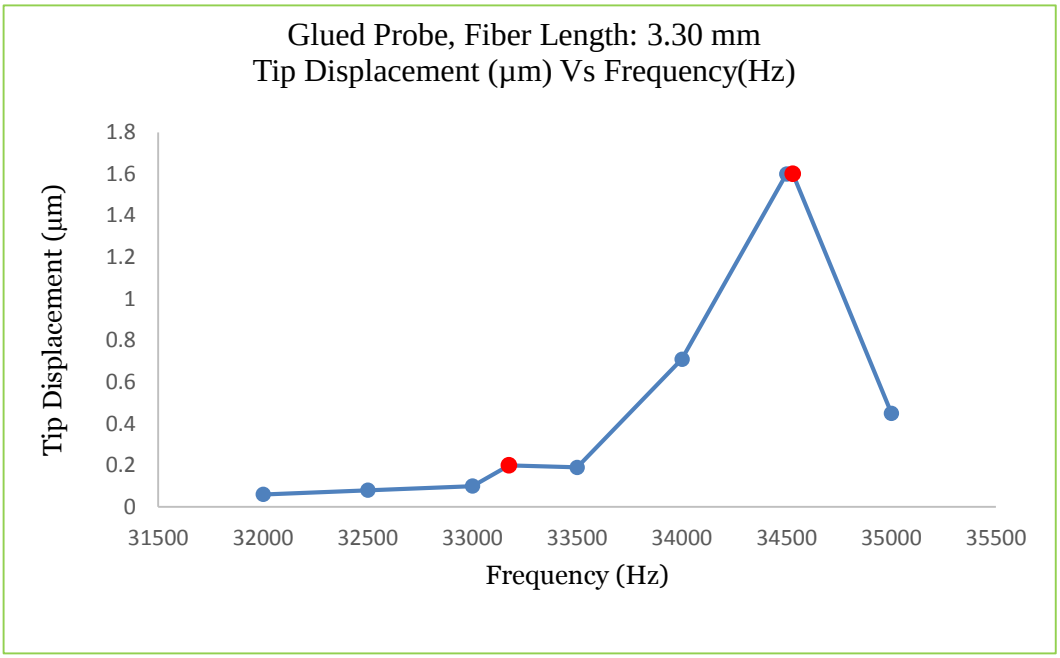

Figure 5.17: Variation in tip displacement with frequency for a glued probe

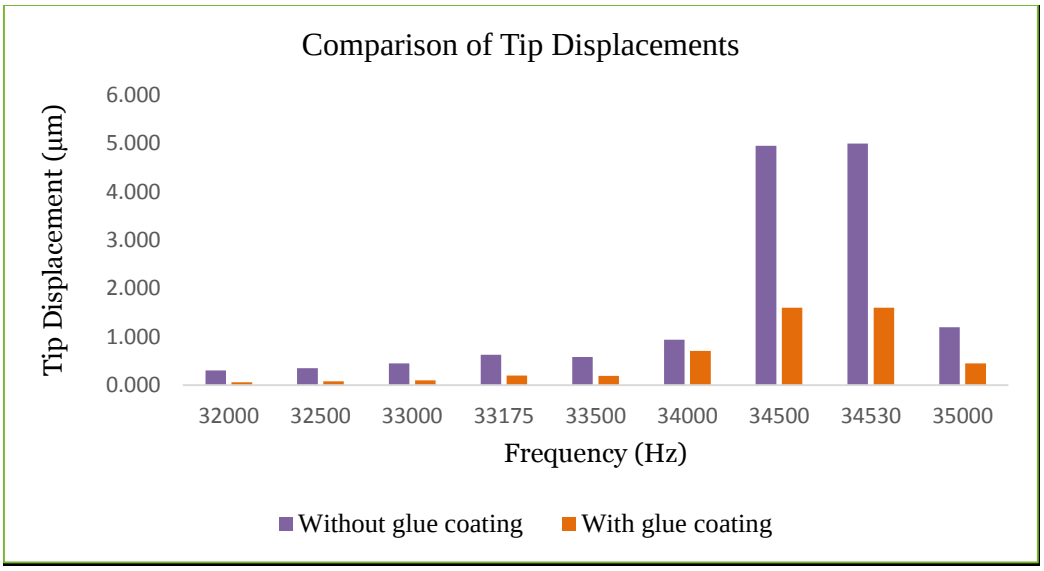

Figure 5.18: Comparison of tip displacements with and without glue coating

It can be seen in the graph 5.18 that the trend of the tip displacement for the glued model is similar to the model not including the glue. The tip displacement is maximum at the resonating frequency. The magnitude, however, is notably smaller than its counterpart. In fact all values of tip displacements for the glue coated probe at different frequencies report less magnitudes than their corresponding counterparts as shown in figure 5.18

CHAPTER 6: RESULTS AND PARAMETRIC STUDIES FOR MODE 4 LOADING

In this chapter, results for the dynamic simulations involving mode 4 type (anti-symmetric) loading of the fork are discussed. A typical plot of the tip displacement in y-direction for the fiber of 3.20 mm length and an excited frequency of 32768 Hz is displayed in figure 6.1. The plot is similar to the symmetric mode loading where the tip undergoes through a transient region before finally achieving an almost steady state.

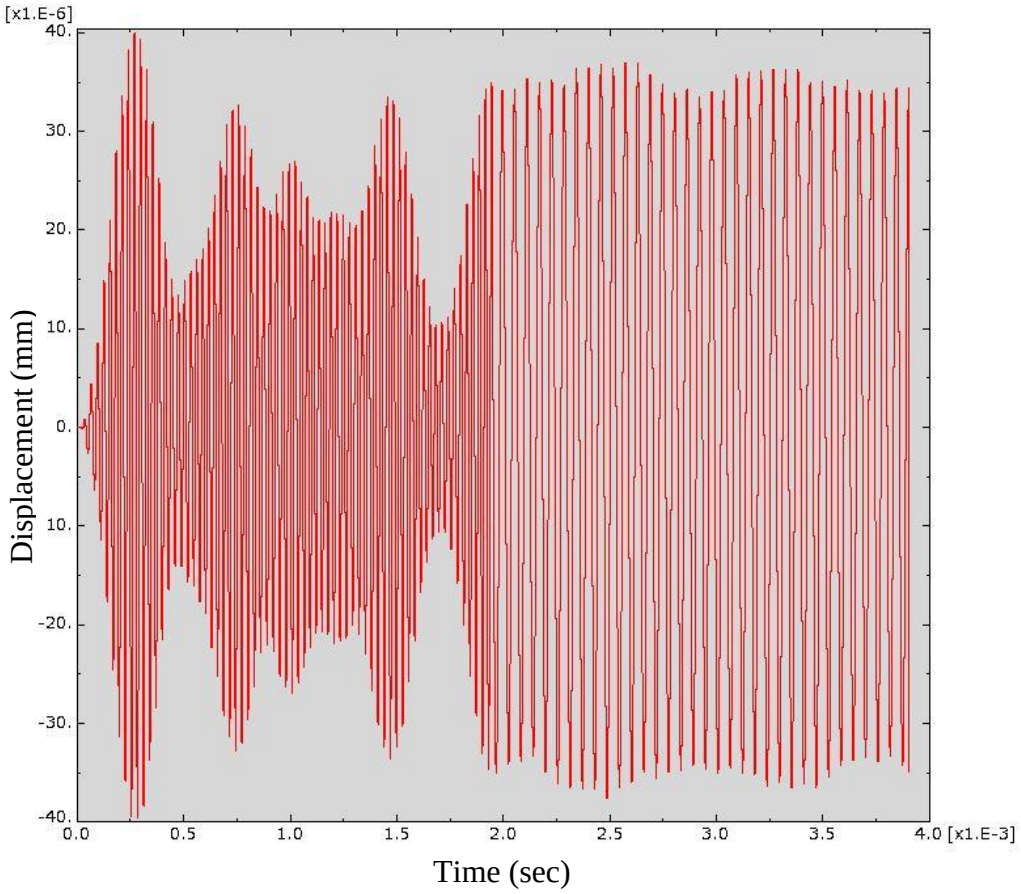

Figure 6.1: Plot of tip displacement with time

6.1 Parametric Studies

As mentioned in the introduction, probe with the mode 4 type of loading is also analyzed for three potentially affecting factors discussed in the subsequent sections.

6.1.1 Length of Fiber

In this case, the probe is excited at a frequency of 32768 Hz and length of the fiber has been varied from 3.20 mm to 3.35 mm with an interval of 0.05 mm. The results for the variation in fiber length are tabulated below:

Table 6.1: Tip displacement in y-direction for different fiber lengths: mode 4 loading

Frequency: 32768 Hz	
Fiber Length (mm)	Tip Displacement (µm)
3.20	0.036
3.25	0.082
3.30	0.560
3.35	0.150

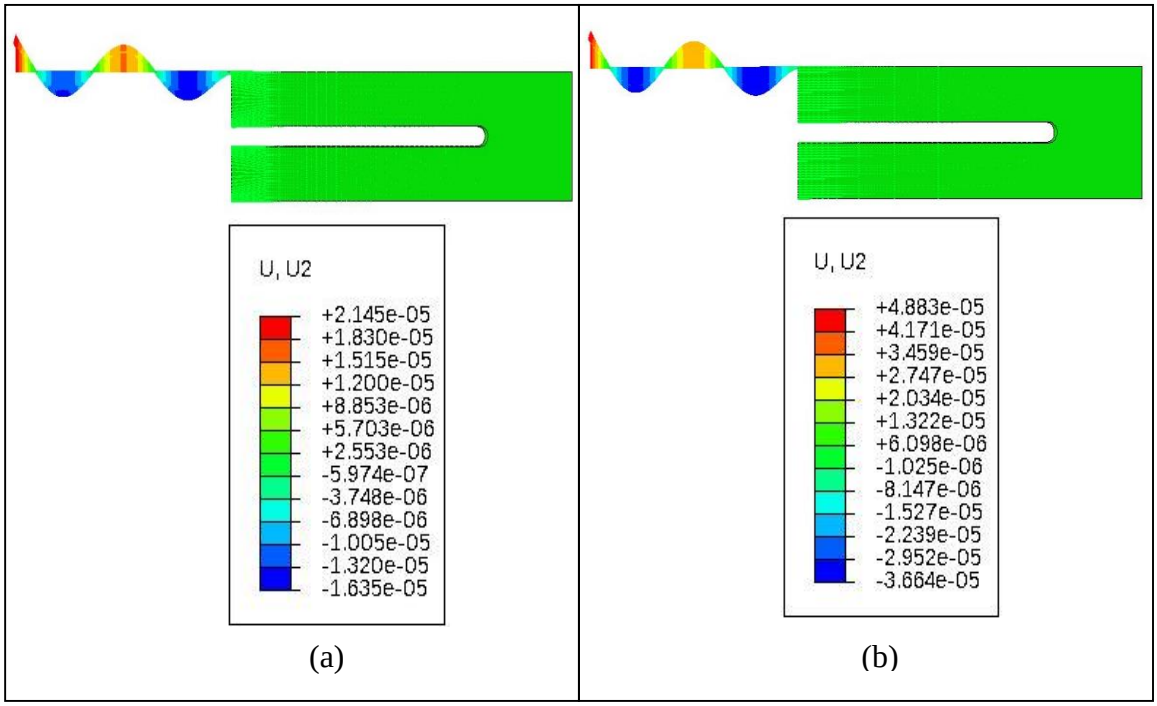

Figure 6.2: Vector displacement of fibers, (a) 3.25 mm, and (b) 3.35 mm at 2.36 milliseconds, in millimeters

It is seen that the maximum tip oscillations occur for 3.30 mm length of the fiber. Figures 6.2 (a) and (b) confirm presence of four nodes along the fiber length. Moreover, tip displacements obtained for a particular fiber length are very close to those obtained with mode 3 type of loading for the respective fiber lengths. The results for both mode 3 and mode 4 type of loading are charted in figure 6.3.

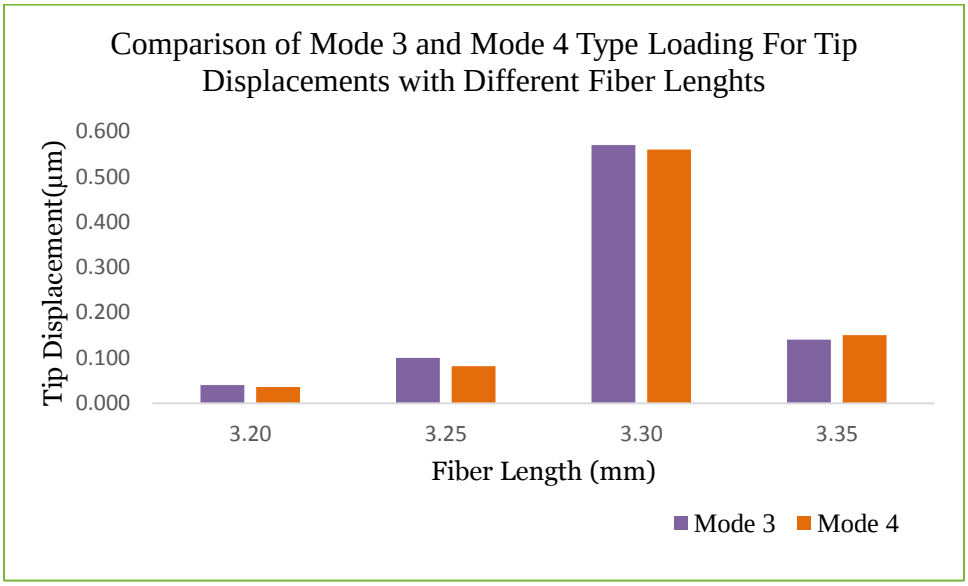

Figure 6.3: Comparison of mode 3 and mode 4 type loading

6.1.2 Effect of Frequency

The probe with 3.35 mm fiber length is studied for the effects of externally excited frequency on the tip oscillations. Table 6.2 shows the results for this parametric study. The tip displacement, again is maximum at the frequency of 34530 Hz. In addition, the values of tip oscillations at different frequencies are barely different from mode 3 type of loading. This is illustrated in charts 6.4, 6.5.

Table 6.2: Effect of frequency on the tip displacement for a probe with 3.35 mm fiber

Fiber Length: 3.35 mm	
Frequency (Hz)	Tip Displacement (μm)
32000	0.080
32768	0.150
33000	0.210
34000	0.250
34530	0.510
35000	0.160

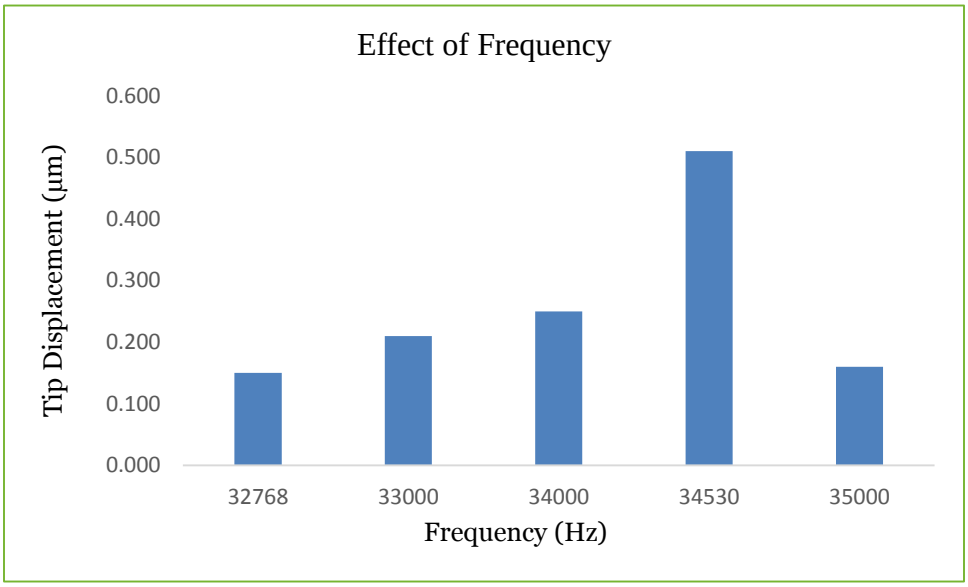

Figure 6.4: Effect of frequency on the fiber tip displacement

A maximum tip displacement of 0.510 μm is obtained at 34530 Hz. It is comparable with 0.535 μm, the tip displacement in mode 3 type of loading. A probe of 3.3 mm fiber length is similarly analyzed at 34530 Hz, and the tip displacement is found to be 4.95 μm, again almost same in magnitude to mode 3 type of loading, which reveals the tip displacement of 5.00 μm.

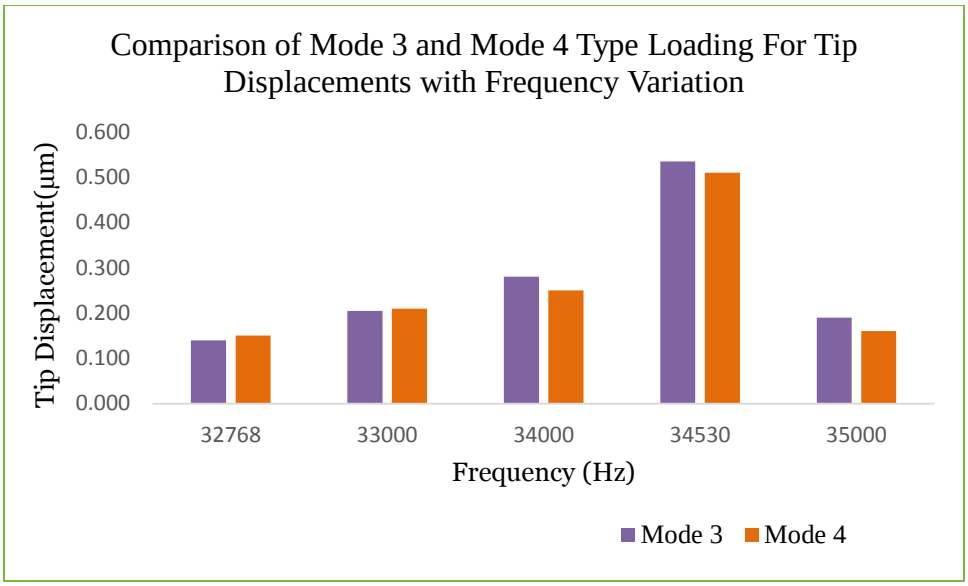

Figure 6.5: Comparison of mode 3 and mode 4 type loading for frequency variation

6.1.3 Effect of Misalignment

The effect of misalignment in mode 4 loading is studied by analyzing 3.30 mm fiber length probe at 32000 Hz. Symmetric and offset-skew scenarios have been considered. Offset-skew position is logical, since it combines the setting of the skew and the offset placements. The results are shown in table 6.3. It is seen again that the misalignment has a minimal effect on the fiber tip oscillation.

A trace of the fiber tip can also be contoured for mode 4 type loading on the similar lines to the trace obtained in chapter 5 for mode 3 loading. The MATLAB 2-d and 3-d plots for symmetric position are illustrated in the figures 6.6 (a) and (b).

Table 6.3: Values of tip displacements for different fiber mounting on the fork

Effect of Misalignment	
Geometry	Tip Displacement (μm)
Symmetric	0.31
Offset-Skew	0.32

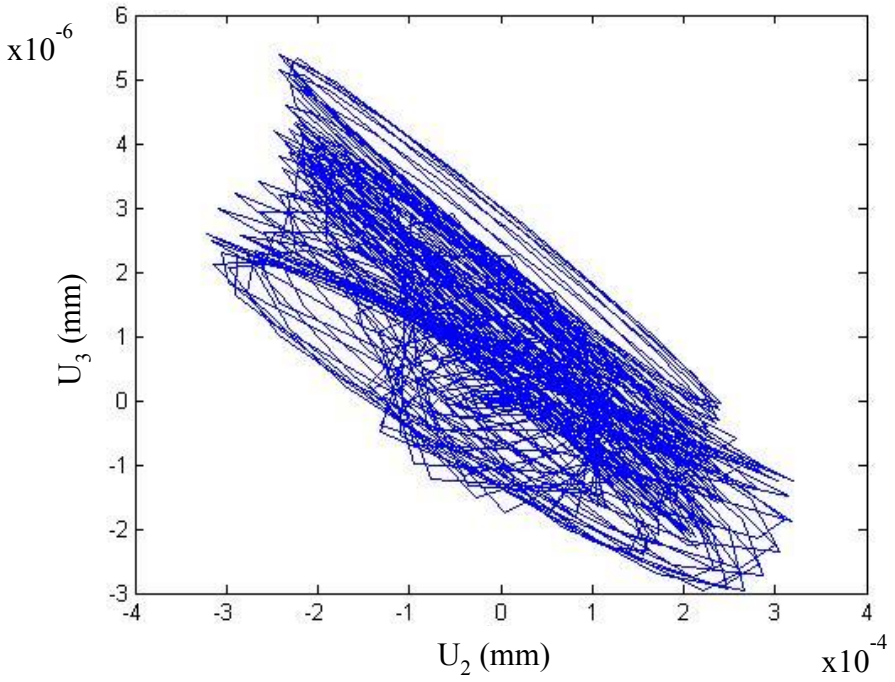

(a)

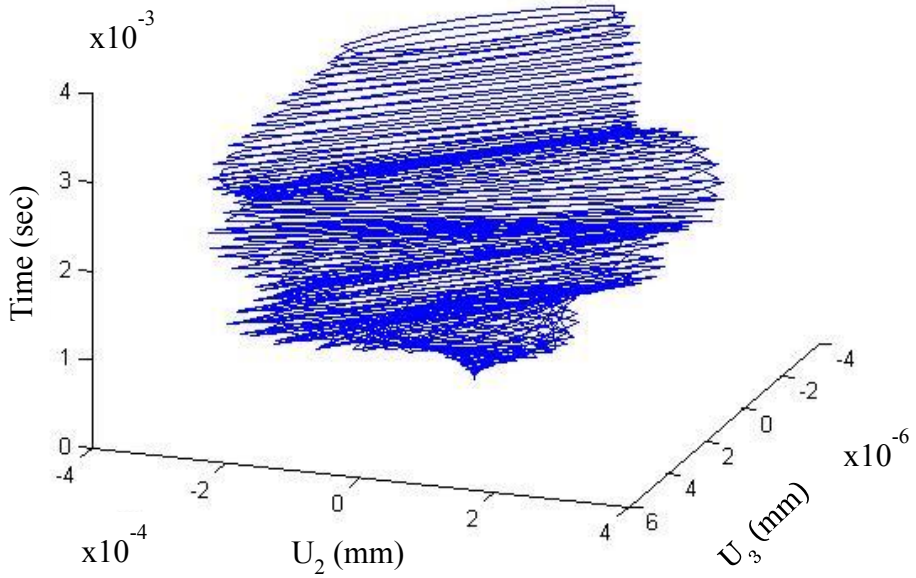

(b)

Figure 6.6 (a), (b): Trace of the fiber tip for symmetric position

6.2 Glue Contact Analysis

Lastly, a layer of glue is modeled in the mode 4 type loading, similar to the studies discussed in chapter 5 to perform the frequency swipe analysis. The probe used for such a study has the fiber length of 3.35 mm. Frequencies of excitation varied in the loading are 33000 Hz to 35000Hz with a spacing of 1000 Hz along with resonant frequency. The results for the tip displacement are summarized in the table 6.4. It can be seen from the figure 6.7 that the maximum tip displacement of 0.19 µm occurs again at 34530 Hz.

Table 6.4: Values of tip displacements for different frequencies of excitation

Glued Probe	
Fiber Length: 3.35 mm	
Frequency (Hz)	Tip Displacement (µm)
33000	0.023
34000	0.080
34530	0.195
35000	0.035

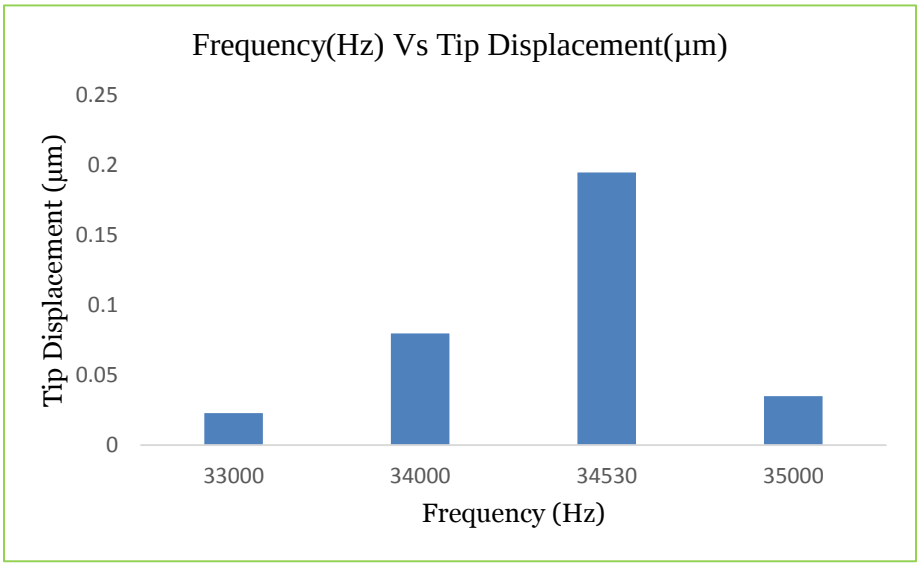

Figure 6.7: Variation in tip displacement with frequency for a glued probe

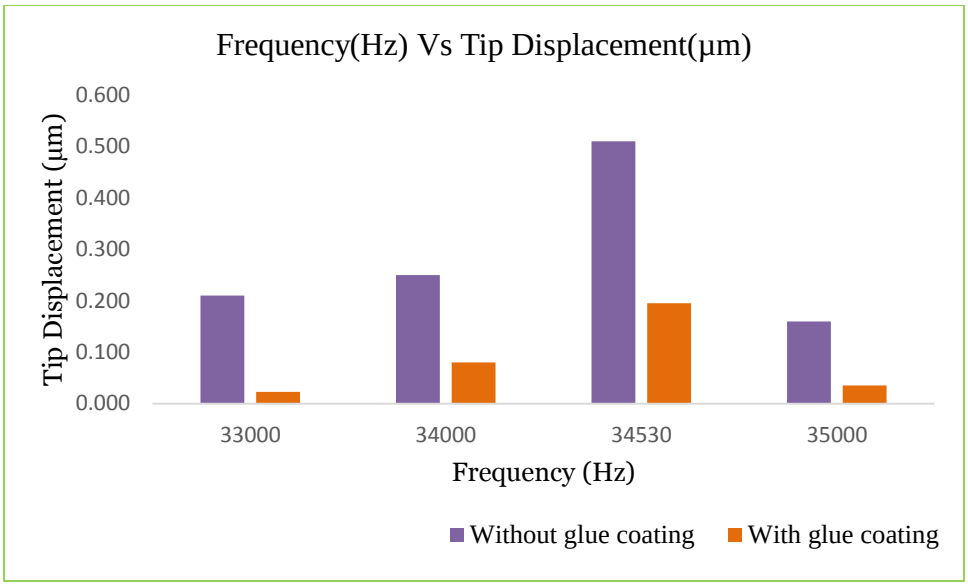

Figure 6.8 Comparison of tip displacements with and without glue coating

Figure 6.8 comparing the values of fiber tip displacements for a range of frequencies with and without glue coating is displayed. Again for mode 4 type loading too, the displacements for the glued probe are significantly less than the probe not including glue.

CHAPTER 7: SUMMARY AND CONCLUSIONS

Fiber tip oscillations occurring in vortex machining are studied in the thesis. The thesis begins with the simple task of a modal analysis of the fork and then the probe. The symmetric and anti-symmetric modes of the fork vibration are found and used in the dynamic simulations for which an Abaqus/Explicit scheme has been employed. The three potential parameters affecting the tip motion are discussed. These parameters are considered in mode three and mode four type loadings. Moreover, a glued model incorporating the Norland Optical Adhesive used to attach the fork and the fiber in experiments is also built in Abaqus and analyzed for a frequency swipe analysis.

It is found that the tip displacement is maximum for a 3.3 mm length of the fiber and a maximum of 5 μm displacement is observed at the resonating frequency. The maximum tip displacement is consistent with both the mode three and the mode four type loadings. Four nodes along the length of the fiber are spotted, validated from the experimental findings. Expectedly, frequency of excitation affects the tip oscillations. However, different placements of the fiber with respect to the fork longitudinal axis hardly alter them. This is again consistent with the experimental observations. Yet, an imperfect contact between the fork and the fiber may affect the fiber tip displacement. Inclusion of the glue significantly influences the tip oscillation and hence must be considered in the finite element models. The fiber tip response with time shows that the transients initially excite with more than one node. This can be seen by the ‘beats’ in the transient region. One of the frequencies then gets damped with time.

The nodes along the fiber length and the misalignment parameters can be easily located in the finite element models, which otherwise are difficult to note due to the tiny geometry of the system. Thus, the thesis provides a good insight to study some potentially influencing factors at a certain computational cost.

The present finite element model can be further expanded to include the slurry part of the vortex machining. This can also help investigate other parameters affecting the tip displacement, such as slurry depth, type of slurry used, etc. If expanded even further, the finite element model can be used to define the vortex machining process, enabling it to analyze parameters, such as fiber tip and workpiece stand-off distance.

REFERENCES

[1] Qin, Yexian, and R. Reifenberger. "Calibrating a tuning fork for use as a scanning probe microscope force sensor." *Review of scientific instruments*78.6 (2007): 063704.

[2] Grober, Robert D., et al. "Fundamental limits to force detection using quartz tuning forks." *Review of Scientific Instruments* 71.7 (2000): 2776-2780.

[3] Edwards, Hal, et al. "Fast, high-resolution atomic force microscopy using a quartz tuning fork as actuator and sensor." *Journal of applied physics* 82.3 (1997): 980-984.

[4] Lee, Sungkyu, et al. "Analytical and finite element method design of quartz tuning fork resonators and experimental test of samples manufactured using photolithography 1-significant design parameters affecting static capacitance." *Vacuum* 75.1 (2004): 57-69.

[5] Friedt, J-M., and E. Carry. "Introduction to the quartz tuning fork." *American Journal of Physics* 75.5 (2007): 415-422.

[6] Kosterev, Anatoliy A., et al. "Applications of quartz tuning forks in spectroscopic gas sensing." *Review of Scientific Instruments* 76.4 (2005): 043105.

[7] Chałupniak, Andrzej, et al. "Application of quartz tuning forks for detection of endotoxins and Gram-negative bacterial cells by monitoring of Limulus Amebocyte Lysate coagulation." *Biosensors and Bioelectronics* 58 (2014): 132-137.

[8] Cho, Nam-Joon, et al. "Quartz resonator signatures under Newtonian liquid loading for initial instrument check." *Journal of colloid and Interface Science*315.1 (2007): 248-254.

[9] Vijayraghavan, K., et al. "Measurement of elastic properties in fluid using high bandwidth atomic force microscope probes." *Applied Physics Letters* 102.10 (2013): 103111.

[10] Zhang, Jian, et al. "Determination of liquid density with a low frequency mechanical sensor based on quartz tuning fork." *Sensors and Actuators B: Chemical* 84.2 (2002): 123-128.

[11] Toledo, J., et al. "Application of quartz tuning forks and extensional microresonators for viscosity and density measurements in oil/fuel mixtures."*Microsystem Technologies* 20.4-5 (2014): 945-953.

[12] Sader, John Elie. "Surface stress induced deflections of cantilever plates with applications to the atomic force microscope: Rectangular plates." *Journal of Applied Physics* 89.5 (2001): 2911-2921.

[13] Bauza, Marcin B., et al. "Development of a virtual probe tip with an application to high aspect ratio microscale features." *Review of scientific instruments* 76.9 (2005): 095112.

[14] Woody, Shane, et al. "Standing wave probes for microassembly." *Review of Scientific Instruments* 79.8 (2008): 085107.

[15] Chesna, Jacob W., et al. "Development of a Micro-scale Assembly Facility with a Three Fingered, Self-aware Assembly Tool and Electro-chemical Etching Capabilities." *Precision Assembly Technologies and Systems*. Springer Berlin Heidelberg, 2012. 1-8.

[16] Hastings, D. J., et al. "A THREE FINGERED HAND FOR A MICRO-ROBOTIC ASSEMBLY SYSTEM."

[17] Nowakowski, B. K., et al. "Chronocoulometry for quantitative control of mass removal in micro-structures and sensors." *Review of Scientific Instruments*83.10 (2012): 105115.

[18] Nowakowski, B. K., et al. "Vortex Machining: Localized Surface Modification Using an Oscillating Fiber Probe." *Machining Science and Technology* 13.4 (2009): 561-570.

[19] J.B. Hunt, "Experimental Investigation of process parameters in vortex machining", Thesis, UNC Charlotte, 2014.

[20] Heyliger, Paul, Hassel Ledbetter, and Sudook Kim. "Elastic constants of natural quartz." The Journal of the Acoustical Society of America 114.2 (2003): 644-650.

[21] Ogi, Hirotsugu, et al. "Elastic, anelastic, and piezoelectric coefficients of α-quartz determined by resonance ultrasound spectroscopy." *Journal of applied physics* 100.5 (2006): 053511.

[22] Brice, J. C. "Crystals for quartz resonators." *Reviews of modern physics* 57.1 (1985): 105.

[23] from goodfellow.com/pdf/842_1111010.pdf

[24] from norlandprod.com/adhesives/NOA%2061.html

[25] Bennighof, Jeffrey K., and Richard B. Lehoucq. "An automated multilevel substructuring method for eigenspace computation in linear elastodynamics."SIAM Journal on Scientific Computing 25.6 (2004): 2084-2106.

[26] Jones, Mark T., and Merrell L. Patrick. The use of Lanczos's method to solve the large generalized symmetric definite eigenvalue problem. No. ICASE-89-69. INSTITUTE

FOR COMPUTER APPLICATIONS IN SCIENCE AND ENGINEERING HAMPTON VA, 1989.

[27] Nguyen, D. T., et al. "Subspace and Lanczos sparse eigen-solvers for finite element structural and electromagnetic applications." Advances in Engineering Software 31.8 (2000): 599-606.

[28] Arbenz, Peter, et al. "A comparison of eigensolvers for large-scale 3D modal analysis using AMG-preconditioned iterative methods." International Journal for Numerical Methods in Engineering 64.2 (2005): 204-236.

[29] Natvig, Jon, G. Nour-Omid, and B. N. Parlett. Effect of the CYBER 205 on methods for computing natural frequencies of structures. No. PAM-218. CALIFORNIA UNIV BERKELEY CENTER FOR PURE AND APPLIED MATHEMATICS, 1984.

[30] Nour-Omid, Bahram, Beresford N. Parlett, and Robert L. Taylor. "Lanczos versus subspace iteration for solution of eigenvalue problems." International journal for numerical methods in engineering 19.6 (1983): 859-871.

[31] Abaqus/Explicit User's Manual, version 6.11

[32] Mangala, Sandhya, et al. "Parallel adaptive simulations of dynamic fracture events." Engineering with Computers 24.4 (2008): 341-358.

[33] from dynasupport.com/tutorial/ls-dyna-users-guide/time-step-size

[34] Liu, G. R., and SS Quek Jerry. "A finite element study of the stress and strain fields of InAs quantum dots embedded in GaAs." Semiconductor science and technology 17.6 (2002): 630.